Materials Today Bio 39 (2026) 103443

Contents lists available at ScienceDirect

Materials Today Bio

journal homepage: www.journals.elsevier.com/materials-today-bio

Redefining 3D cell culture: Human methacryloyl platelet lysates hydrogels for reliable, consistent, and ethical applications

Mariana M. Dias [a,b], Ana T. Rufino [a], Rui Vitorino [c], Catarina A. Custódio [a,b,*], João F. Mano [a,b,**]

[a] Metatissue, PCI - Creative Science Park, Via Do Conhecimento, Ílhavo, Portugal
[b] CICECO – Aveiro Institute of Materials, Department of Chemistry, University of Aveiro, Aveiro, Portugal
[c] IBiMED, Department of Medical Sciences, University of Aveiro, Aveiro, Portugal

ARTICLE INFO

Keywords:
Human methacryloyl platelet lysates (hPLMA)
Matrigel
Xeno-free
Hydrogels
Transcriptomic analysis
Immunogenicity

ABSTRACT

The transition to human-derived biomaterials is critical for advancing ethical and clinically relevant three-dimensional (3D) cell culture systems. In this study, we evaluate the performance of human methacryloyl platelet lysates (hPLMA), a xeno-free, human-derived hydrogel, benchmarking it against Matrigel, the gold standard in the field, and a widely used but animal-derived matrix with an unethical tumor origin. Human adipose-derived stem cells (hASCs) were encapsulated in both materials and cultured for 14 days. Both materials support high viability and proliferation for 7 days. However, hPLMA promotes consistent cell growth and intricate networks, while Matrigel induces rapid spreading, leading to massive cell clusters and ultimately the degradation of the hydrogel after 7 days. Although macrophage culture in both materials show low cytokine levels, the transcriptomic profile of hASCs in Matrigel reveal a constant high expression of immune-related genes, especially after 5 days. In contrast, hASCs in hPLMA have lower expression of immune response genes and higher expression of genes associated with cell migration, adhesion, and matrix organization, showing hPLMA's ability to mimic the natural cell environment. These results position hPLMA as a robust, xeno-free platform not only for 3D cell culture applications such as drug screening, organ-on-chip and tissue models, but also as a promising candidate for therapeutic applications, including tissue engineering and regenerative medicine. Ultimately, its human origin enhances physiological relevance while minimizing immune activation, supporting its translation towards clinical use.

1. Introduction

A long portfolio has been proposed to support cell culture, evolving from the simple two-dimensional (2D) cultures, such as glass and polystyrene, to the more advanced three-dimensional (3D) systems, including hydrogels and decellularized tissues. Although 2D systems are easier to use and affordable, they cannot reproduce key features of native tissues, such as heterogeneous mechanical stiffness, spatial cell organization, biochemical gradients, and complex cell–cell communication [1]. In contrast, 3D cultures allow cell-matrix and cell-cell adhesion in multiple directions, which improves cell communication. Different synthetic polymers, natural biomaterials, and semisynthetic composites have been explored to mimic the physiological conditions. Still, among the natural biomaterials, Matrigel has remained the golden standard for 3D cell culture for half a century. Matrigel can effectively mimic the biochemical properties of the native extracellular matrix (ECM) due to its composition of proteins (e.g., laminin, collagen IV, entactin), growth factors (GFs), and enzymes, derived from the basement membrane of the Engelbreth-Holm-Swarm (EHS) mouse sarcoma [2]. Thus, Matrigel has been used for several applications, including cell culture, cell differentiation, and spheroid and organoid encapsulation [3]. Despite being a cost-effective option for 3D cell cultures, Matrigel has significant limitations due to its animal tumor origin. The production of a single standard Matrigel vial necessitates the continuous growth of tumors in two mice. Consequently, the animals employed in Matrigel manufacturing undergo tumor development throughout their lifespan [4]. Beyond the evident ethical concerns associated with this process, the xenogeneic composition of Matrigel may also elicit

* Corresponding author. Metatissue, PCI - Creative Science Park, Via Do Conhecimento, Ílhavo, Portugal
** Corresponding author. Metatissue, PCI - Creative Science Park, Via Do Conhecimento, Ílhavo, Portugal
E-mail addresses: catarinacustodio@ua.pt (C.A. Custódio), jmano@ua.pt (J.F. Mano).

https://doi.org/10.1016/j.mtbio.2026.103443
Received 7 May 2026; Received in revised form 29 June 2026; Accepted 9 July 2026
Available online 9 July 2026

immunogenic responses in cultured cells [5,6]. Consequently, this limits Matrigel's applications and hinders the translation of its results to clinics. However, Matrigel is still widely applied in research, and it is stated in some differentiation protocols [7]. Even so, it is well documented that Matrigel's complex and undefined composition leads to high batch-to-batch variability and poor reproducibility, complicating the interpretation of results from assays that use this material [8,9]. In fact, Matrigel even has trace amounts of DNA and RNA, which have been shown to influence cell analysis [10].

In recent years, human and synthetic alternatives to animal-based matrices have been proposed as a way to reduce the use of animals and animal-derived products in research. Particularly in clinical research, human-derived proteins have been extensively studied due to their higher biocompatibility and ability to mimic native human tissues [11]. For example, human decellularized liver has been used for ECM scaffolds, as it contains several proteins, such as collagens and fibronectin, that mimic native liver. Effectively, Mazza et al. demonstrated that it is possible to culture different human hepatocytes in liver scaffolds, thereby helping the repopulation of the decellularized tissue [12]. Furthermore, human ECM derived from the amniotic membrane has recently emerged as a promising biomaterial platform for applications in cell culture and neural tissue regeneration [13,14].

Another widely available and easily obtainable human-derived material is platelet lysates (hPL) derived from human blood, which has proven effective as a supplement for culture media. The abundant presence of albumin, fibronectin, and GFs in hPL enhances cell proliferation, adhesion, and differentiation across multiple cell types when compared with traditional fetal bovine serum (FBS) supplementation [15]. Moreover, hPL exhibits reduced risks of immunogenicity, viral and mycoplasma contamination, and features lower batch-to-batch variability than animal-derived products such as FBS [16]. These advantages result from its production under standardized human blood processing protocols. Nevertheless, despite its favorable biochemical composition, hPL lacks intrinsic mechanical properties and therefore cannot form or support a hydrogel structure.

A commercially available formulation of the hPL is the methacryloyl human platelet lysates (hPLMA, Metatissue®), which have shown the ability to enhance the mechanical robustness and processability of hPL-based materials [17]. Indeed, several studies have shown the effectiveness of this chemical modification, since it preserves the proteins and bioactive molecules naturally present in hPL, such as albumins, platelet-derived growth factor (PDGF), and vascular endothelial growth factor (VEGF), while enabling the preparation of stable hydrogels that allow for more than 14 days of cell culture [17,18]. Even though hPLMA hydrogels' stiffness is typically higher than Matrigel, a myriad of cell types have already been cultured in hPLMA, including mouse fibroblasts, human adipose stem cells and mesenchymal stem cells, human umbilical vein endothelial cells, human osteosarcoma cell lines, human epithelial cell lines, macrophages and cardiomyocytes, to name a few [17–21]. Moreover, hPLMA properties, such as stiffness and porosity, can be easily tuned by altering the degree of methacrylation and hPLMA concentration [17]. For instance, hPLMA hydrogels were previously compared with Matrigel regarding tumor spheroids invasion, showing higher invasion kinetics, controlled by hPLMA stiffness [21]. For these reasons, we hypothesize that hPLMA can offer a more accurate matrix for human cell cultures than Matrigel, exhibiting lower batch-to-batch variability that enhances reproducibility. This could improve the translatability of in vitro studies to clinical outcomes while reducing reliance on animal-derived materials and promoting ethical research practices. Therefore, in this study, we present for the first time a comprehensive comparison between hPLMA and Matrigel, focusing on cellular responses, including proliferation, morphology, metabolic activity, and transcriptomic profiles following encapsulation, as well as the immunogenicity and cytotoxicity of the respective materials.

2. Results and discussion

In human research, it is particularly important to implement human-derived matrices that closely recapitulate the biochemical and mechanical properties of native human tissues, thereby enabling more physiologically relevant and reproducible experimental outcomes. In this study, we conducted a systematic comparison of the commercially available products hPLMA (Metatissue®, Portugal), a human protein-derived matrix, and Matrigel (Corning, USA) to determine whether hPLMA has the potential to replace this widely used animal-derived standard in 3D cell culture applications.

2.1. Biological characterization

Human adipose-derived stem cells (hASCs) activity was chosen to evaluate and compare the cell performance in hPLMA and Matrigel hydrogels, focusing on their described ability to adhere, grow and proliferate in these matrices. Cell culture conditions were also chosen based on the literature description as the best conditions for both matrices. Thus, hASCs were encapsulated in hPLMA hydrogels at 15% (w/v) and Matrigel hydrogels at 1.2% (w/v), both concentrations being adequate for hASCs growth [17,22]. Also, considering the extensive degradation of the Matrigel after 7 days, cells were cultured encapsulated within the hydrogels for that maximum period. At the time points 1, 3 and 7 days, hASCs' viability was analyzed through a Live/Dead assay. Overall, hASCs remained viable throughout the 7-day culture in both hPLMA and Matrigel hydrogels, as shown in Fig. 1A.

To analyze cell morphology, DAPI/Phalloidin staining was also performed at the time points 0, 3 and 7 days. In hPLMA hydrogels, hASCs began to spread by day 3, and after 7 days, they were fully elongated with protrusions and extensively connected with surrounding cells, resulting in an intricate network (Fig. 1B). The cells also show actin filaments with a longitudinal arrangement and small protrusions at the cells' ends. This growth pattern is consistent with previous research on hASCs encapsulated in hPLMA and demonstrates that hASCs grow well in these hydrogels, even though they take a longer time to elongate in hPLMA than in Matrigel [23,24]. Right after encapsulation, i.e., at day 0 time point, hASCs were evenly distributed in both materials, presenting a round shape (Fig. 1B). However, when embedded in Matrigel, hASCs start to cluster over time, resulting in large cell aggregates after 7 days of culture. It is also noticeable that a few cells have a very elongated morphology and work as a bridge between clusters. The degradation of Matrigel hydrogels after 7 days may also contribute to the formation of these clusters, allowing cells to sustain themselves as they lose the support of the matrix. Additionally, previous studies have indicated that other cell types, such as fibroblasts, also grow in aggregates when cultured in Matrigel, while adopting an elongated shape in other matrices [25]. Hence, this behavior could also be associated with Matrigel components coupled with its characteristically low stiffness and limited mechanical stability under in vitro conditions. Furthermore, Fig. 1A shows a considerable amount of dead cells within the clusters formed by day 7. These dense aggregates may hinder nutrient and gas exchange, leading to cell death, similar to the formation of a necrotic core, which is characteristic of spheroids and tumors. These differences in hASCs organization inside the hydrogels can also be associated with the matrix stiffness. hPLMA hydrogels at 15% (w/v) have a Young's modulus ranging from 15 to 20 kPa, whereas Matrigel hydrogels at 1.2% (w/v) have a significantly lower Young's modulus of 450 Pa [21,26]. Previous studies have indicated that hASCs proliferate more effectively in hPLMA hydrogels at 15% (w/v) compared to those at 10% (w/v), suggesting that some level of stiffness is beneficial for supporting hASCs growth [17]. However, the higher stiffness of hPLMA hydrogels may slow the cells' initial migration and morphological organization when compared to Matrigel. The softer properties of Matrigel hydrogels facilitate the cells and ECM remodeling, accelerating their growth and proliferation [27].

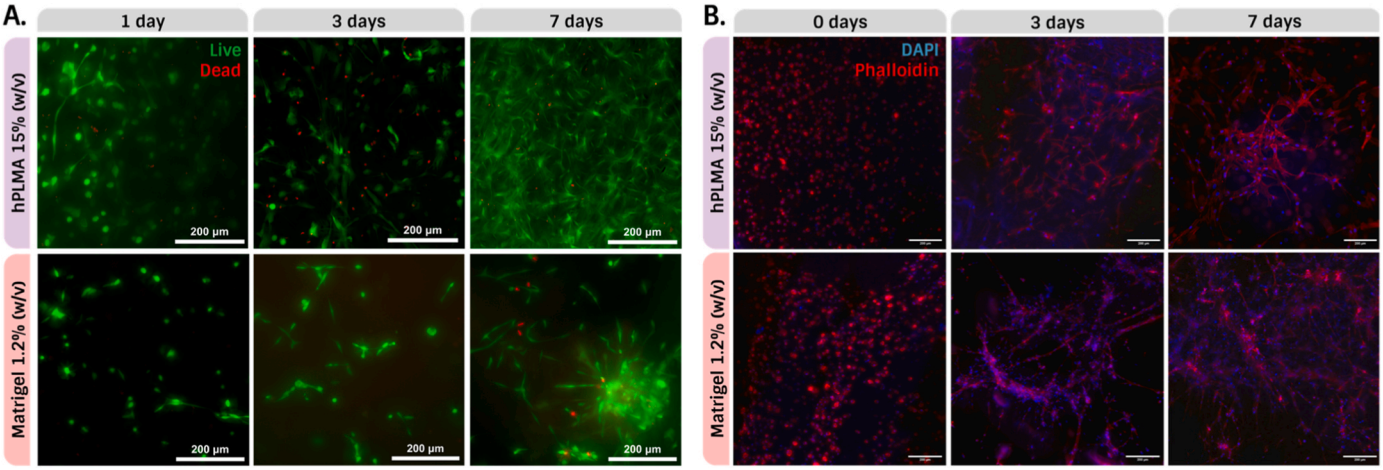

Fig. 1. Representative fluorescence images of hASCs encapsulated in hPLMA and Matrigel hydrogels. The live/dead staining was performed at 1, 3, and 7 days of culture, with calcein AM staining live cells (green) and PI staining dead cells (red). (**A.**) The DAPI/phalloidin staining was performed at 0, 3, and 7 days of culture, with DAPI staining cell nucleus (blue) and phalloidin staining actin filaments (red). (**B.**) Scale bar: 200 µm. (For interpretation of the references to colour in this figure legend, the reader is referred to the Web version of this article.)

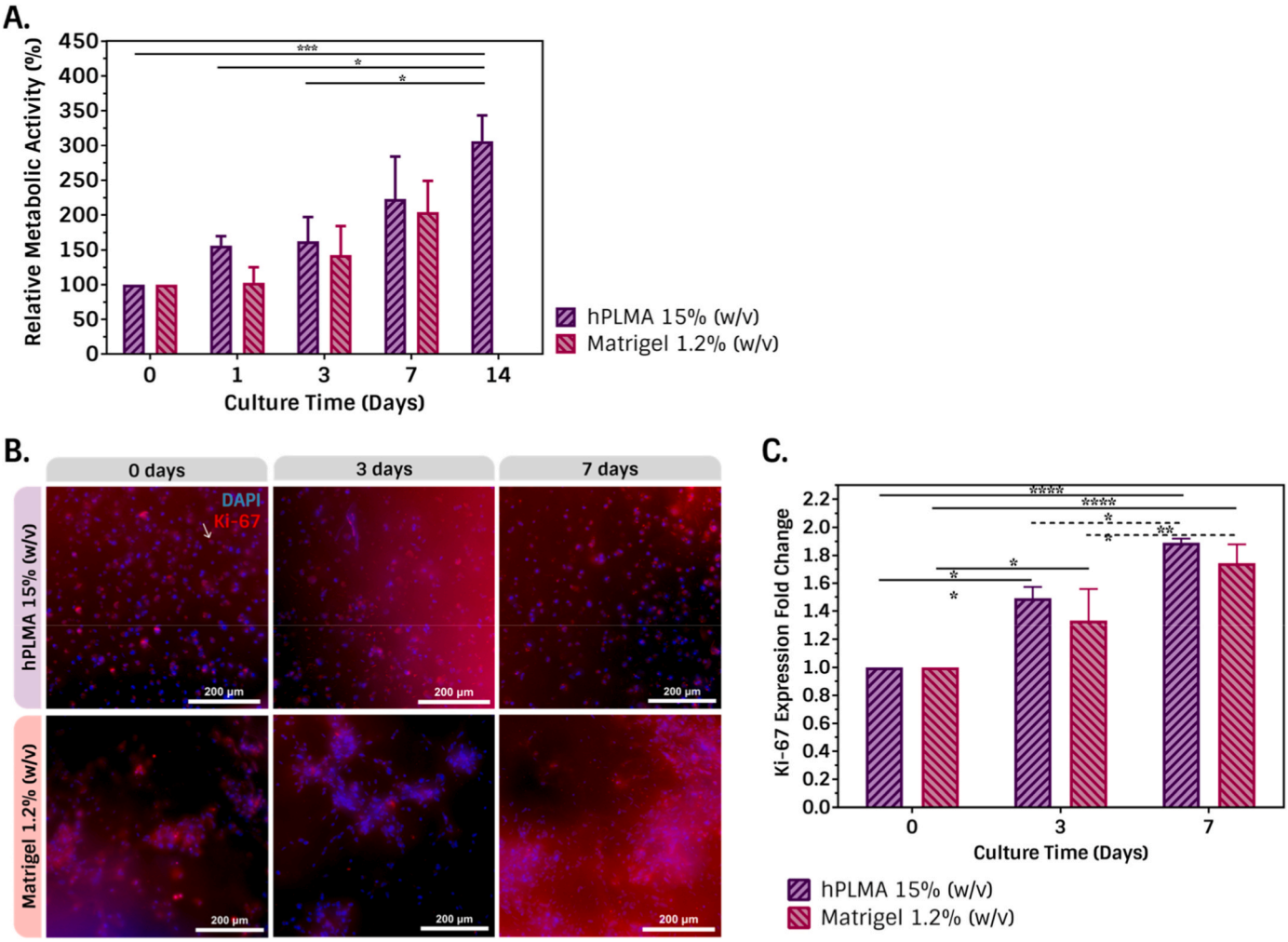

Fig. 2. hASCs' relative metabolic activity in hPLMA and Matrigel hydrogels for five time points, assessed through the CCK-8 assay. Results are expressed as mean (SD) with n = 5 (**A.**) Representative fluorescence images of hASCs encapsulated in hPLMA and Matrigel hydrogels. The DAPI/Ki-67 staining was performed at 0, 3, and 7 days of culture, with Ki-67 expression (red) and DAPI staining cells' nucleus (blue). The white arrow points to an example of Ki-67 stained cells. Scale bar: 200 µm. (**B.**) Fold change in Ki-67 expression calculated from the CTCF equation using the fluorescence images of Ki-67 expression cultured for 3 and 7 days. The fold change is here compared to day 0. (**C.**) Results are expressed as mean (SD) with n = 3. * p-value <0.05, ** p-value <0.01, *** p-value <0.001 and **** p-value <0.0001. (For interpretation of the references to colour in this figure legend, the reader is referred to the Web version of this article.)

Ultimately, hASCs successfully adhered to and proliferated within both matrices, as anticipated given their protein-rich compositions that promote cell–matrix interactions. For example, hPLMA composition includes vitronectin, a human adhesion protein containing RGD motifs that facilitate integrin-mediated attachment, whereas Matrigel is composed primarily of laminin, collagens, and heparan sulfate proteoglycans [17,28]. Despite the slightly delayed cell elongation observed in hPLMA, hASCs exhibited robust growth and a morphology comparable to that typically seen in other 3D matrix systems. These findings demonstrate that hPLMA can effectively support hASCs culture, achieving performance equivalent to Matrigel in sustaining cell adhesion, spreading, and proliferation [29].

The metabolic activity of hASCs was determined at 1, 3, 7 and 14 days of culture using the CCK-8 assay, and the results for each material were normalized to represent the relative metabolic activity compared to day 0. Fig. 2A shows that hASCs have a continuous growth throughout the culture period in both hPLMA and Matrigel, without statistically significant differences between the materials. Nonetheless, it is visible that after 3 days of culture, the growth of hASCs in hPLMA hydrogels has a non-significant 20% greater increase compared to Matrigel hydrogels (162% ± 60 in hPLMA vs. 142% ± 83 in Matrigel). After 7 days of culture, this non-significant 20% difference in metabolic activity prevails (223% ± 86 in hPLMA vs. 205% ± 78 in Matrigel). Finally, after 14 days of culture, there is a triple fold in metabolic activity of hASCs in hPLMA hydrogels (306% ± 74), demonstrating a significant increase compared to 0, 1, and 3 days of culture. In contrast, it was not possible to collect the 14-day time point for Matrigel cultures due to hydrogel degradation, which resulted in cell attachment to the culture plate. Although some studies report that cells can be maintained in Matrigel for up to 14 or even 21 days, these typically employ lower initial cell densities. Other reports have similarly observed that Matrigel hydrogels (30 μL) undergo substantial degradation after only 7 days of culture [30–32]. Moreover, it is well reported that Matrigel degradation is inconsistent and influenced by factors such as batch-to-batch variability, cell density, and enzymes secreted by the cells. In particular, Wong et al. demonstrated that both cell density and culture time significantly affect Matrigel degradation [33]. Another key point influencing Matrigel's degradation is the rate of activity of matrix metalloproteinases (MMPs) and their inhibitors. As previously reported, TIMPs can attenuate Matrigel's degradation, highlighting the critical regulatory role of MMPs in the process [33]. Since type IV collagen is one of the main components of the adipose tissue ECM, hASCs naturally secrete several MMPs to remodel their matrix, particularly MMP-2 and MMP-9, which are type IV collagenases [34]. Consequently, the high type IV collagen content of Matrigel likely makes it particularly susceptible to degradation in the presence of cells such as hASCs. Moreover, prior studies have confirmed the presence of these MMPs and other proteinases in Matrigel, indicating that the matrix itself can affect its degradation and cell-matrix interactions [35]. In the context of long-term cell culture, hPLMA demonstrated a clear advantage over Matrigel, supporting sustained cell growth for up to 14 days without visible signs of structural degradation. This stability is consistent with previous reports showing that hPLMA hydrogels can maintain high cell viability for up to 24 days in culture, reinforcing their suitability for long-term 3D cell culture applications [36].

To further confirm cell proliferation and metabolic activity within both matrices, Ki-67, a nuclear antigen selectively expressed during active phases of the cell cycle, was evaluated as a marker of active cell cycle. The Ki-67 expression was assessed by immunocytochemistry at three time points, specifically 0, 3, and 7 days of culture, in order to determine hASCs' proliferation inside the hydrogels. Overall, there is a noticeable increase in Ki-67 staining throughout the culture time in both materials (Fig. 2B), which is consistent with the cell growth results. The corrected total cell fluorescence (CTCF) (**Equation I**) was used to quantify the changes in Ki-67 expression throughout the culture period, enabling an accurate subtraction of background signal from the fluorescent images. The mean CTCF of each time point was then compared to day 0 to determine the fold change in Ki-67 expression. In Fig. 2C, it is possible to observe a significant increase in Ki-67 expression of hASCs embedded in Matrigel, after 3 and 7 days, with a fold change of 1.33 ± 0.23 at day 3 and 1.74 ± 0.13 at day 7, compared to day 0. Regarding hPLMA hydrogels, hASCs had a significant fold change of 1.49 ± 0.08 after 3 days and 1.89 ± 0.03 after 7 days, compared to day 0. This suggests that hASCs' proliferation rate doubled after a 7-day culture, which is consistent with the metabolic activity results. While there were no significant differences in Ki-67 expression between hPLMA and Matrigel hydrogels, both matrices also had a significant increase in the antigen expression from the third to the seventh day of culture.

These findings, together with the observed metabolic activity results, demonstrate that both hPLMA and Matrigel hydrogels provide a supportive microenvironment for hASCs' growth. Interestingly, hASCs show a tendency for higher cell proliferation and metabolic activity when embedded in hPLMA hydrogels. This fact is likely linked to the GFs released by hPLMA, including VEGF (300-400 pg mL^{-1}) and PDGF (8-10 pg mL^{-1}), which are known to improve cell growth and proliferation [37]. In contrast, although Matrigel is also rich in several GFs (e.g., 5-7.5 ng mL^{-1} of VEGF and 5 - 48 pg mL^{-1} of PDGF), they vary significantly between batches [8,38]. Proteomic analyses of growth factor-reduced Matrigel have revealed the presence of hundreds of additional proteins beyond those typically reported for this product, highlighting its inherent variability, contributing to the complicated interpretation of cellular responses and misleading conclusions in experimental assays [39]. We also tested this variability by analyzing the metabolic activity and viability of hASCs encapsulated in hPLMA and Matrigel hydrogels from different batches. The metabolic activity was not statistically different between the Matrigel batches (Fig. 3). However, batches 1 and 2 at day 3 and batch 1 at day 7 showed coefficients of variation (CV) between 21 and 24% (Table S.1), which indicates considerable variability. In contrast, batch 2 at day 7 and batch 3 at day 3 exhibited poor CV (between 35 and 51%), reflecting high variability among data points. Additionally, the live/dead data (Fig. 4) showed different growth patterns between the Matrigel lots, all resulting in dense cell clusters by day 7. In contrast, hPLMA hydrogels demonstrated more consistent metabolic activity and cell growth across batches. Only two time points showed higher CV, between 23 and 28% (namely, batch 2 at days 1 and 7), which remained within the acceptable range. This proves that, despite having a diverse mixture of human proteins, hPLMA allows consistent cell performance between distinct batches.

Overall, hASCs' biological characterization when encapsulated in hPLMA and Matrigel hydrogels revealed distinct cell-matrix interactions. In Matrigel, hASCs exhibited rapid initial proliferation and extensive matrix remodeling, reflecting the matrix's permissive and compliant nature. In contrast, hASCs in hPLMA hydrogels initially showed limited stretching, consistent with the higher stiffness of this matrix, and its reduced susceptibility to MMPs-mediated degradation compared to Matrigel. Nevertheless, hPLMA supported enhanced metabolic activity and proliferation over time. Additionally, hPLMA hydrogels facilitate the formation of a more dispersed and uniform cell network, contrasting with the cell aggregates in Matrigel. These findings indicate that hPLMA provides a microenvironment conducive to a prolonged and effective hASCs cell growth, which ultimately supports a sustained 3D cell culture compared with Matrigel.

2.2. *hPLMA and Matrigel's immunogenic profile evaluation*

Building on the observed differences in hASCs' behavior, we proceeded to evaluate the immunogenic properties of hPLMA and Matrigel, aiming to determine their suitability for safe and effective 3D cell culture applications. Matrigel's potential immunogenicity and zoonotic contamination have always been a concern [40,41]. Still, it is difficult to find original research that verifies these claims. Therefore, this

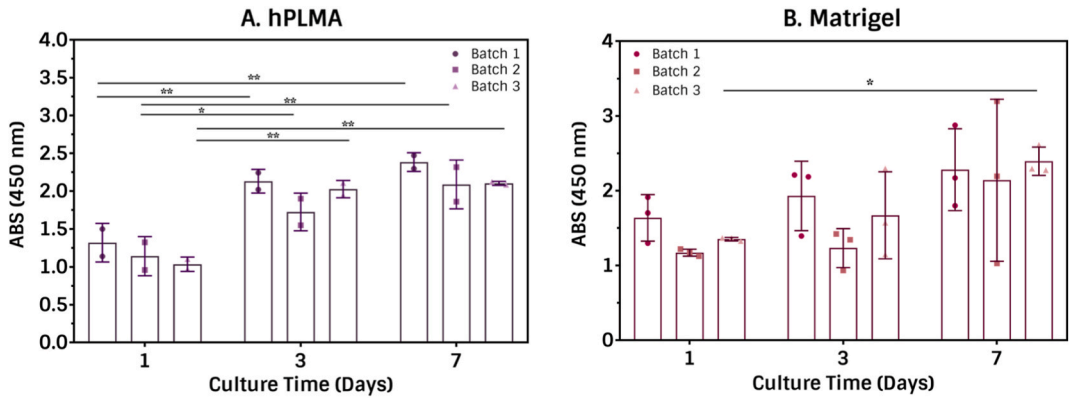

Fig. 3. Metabolic activity of hASCs encapsulated in hPLMA (**A.**) and Matrigel (**B.**) hydrogels from three different batches. Three time points (1, 3 and 7 days) were analyzed through the CCK-8 assay. Results are expressed as mean (SD) with n = 3. * p-value <0.05 and ** p-value <0.01.

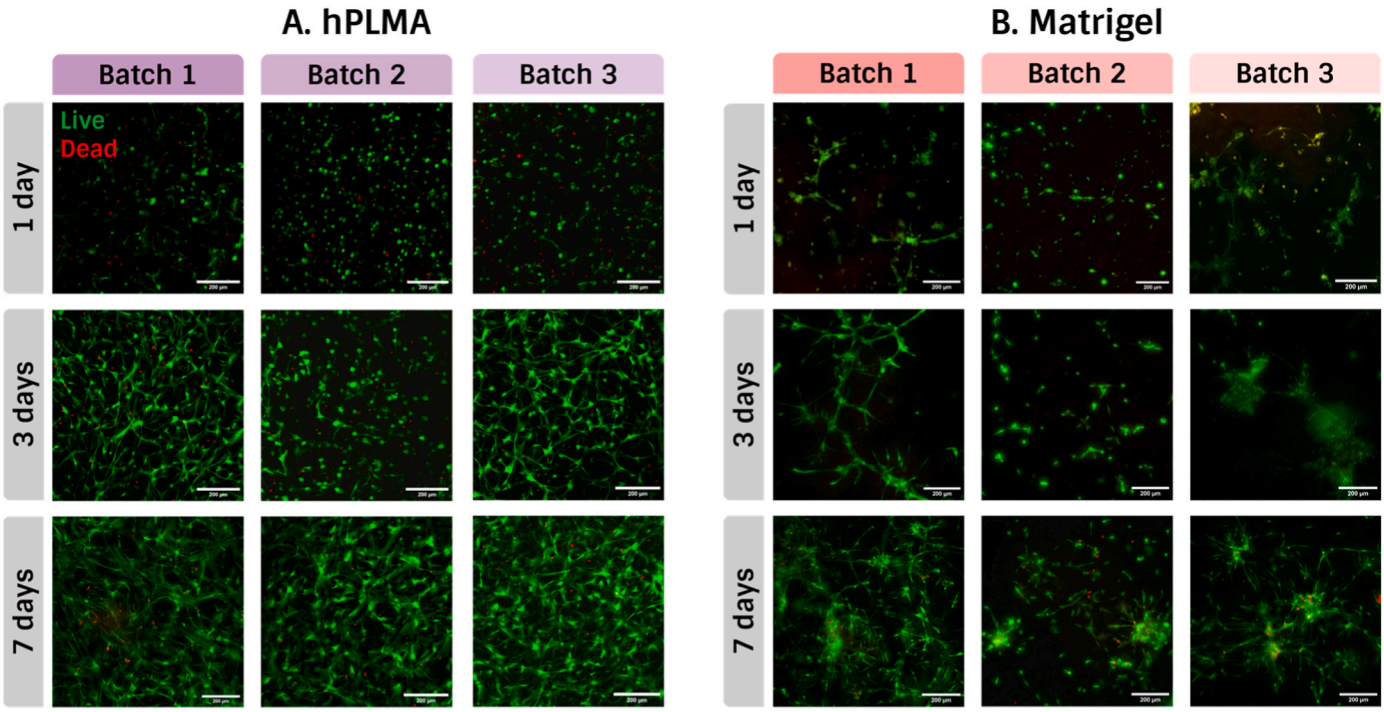

Fig. 4. Representative fluorescence images of hASCs encapsulated in hPLMA (**A.**) and Matrigel (**B.**) hydrogels from three different batches. The live/dead staining was performed at 1, 3, and 7 days of culture, with calcein AM staining live cells (green) and PI staining dead cells (red). Scale bar: 200 μm. (For interpretation of the references to colour in this figure legend, the reader is referred to the Web version of this article.)

represents a significant gap in knowledge that needs to be addressed, especially given the extensive use of Matrigel in 3D cell culture systems. To evaluate whether hPLMA and Matrigel hydrogels trigger an immune response, a monocytic cell line, specifically the THP-1 human monocytes, was differentiated into macrophages and exposed to these matrices.

The activation of an immune response was assessed through quantification of cytokine levels in the culture media. For this, the culture medium of M0, M1, and M2 macrophages was collected after the third and seventh days of culture. Afterwards, the expression of TNF-α, IL-6, and IL-10 was quantified by ELISA assays, and the results are shown in Fig. 5. Previous research has indicated that the differentiation of THP-1 cells into M1 macrophages induces an increase in pro-inflammatory cytokines, namely TNF-α and IL-6, while M2 macrophages have higher levels of anti-inflammatory cytokines, such as IL-10 [42]. Our results demonstrate that, at day 3, M1 macrophages had a basal expression of TNF-α in both materials (4.00 ± 1.70 pg mL^{-1} in hPLMA vs. 2.43 ± 0.92 pg mL^{-1} in Matrigel), and this expression significantly decreased after 7 days. Regarding IL-6 expression, only M1 macrophages in contact with Matrigel had minimal levels of this cytokine at day 3 (3.28 ± 2.81 pg mL^{-1}), which was significantly higher compared to the expression at day 7 (1.22 ± 0.43 pg mL^{-1}). Equally, for IL-10, only Matrigel had a low expression of this cytokine at the third day (2.13 ± 0.22 pg mL^{-1}), which was significantly reduced at the seventh day of culture.

Thus, within this experimental model, neither hPLMA nor Matrigel hydrogels appear to elicit detectable pro-inflammatory or anti-inflammatory responses. Across all conditions and time points, the cytokines' expression remained at baseline levels, below 6 pg mL^{-1}, consistent with physiological concentrations in healthy human subjects [43]. This outcome was expected for hPLMA, given its human-derived origin and primary composition of serum albumin, a well-characterized non-immunogenic protein [44]. Consistently, previous research using methacrylated matrices, such as GelMA, has reported

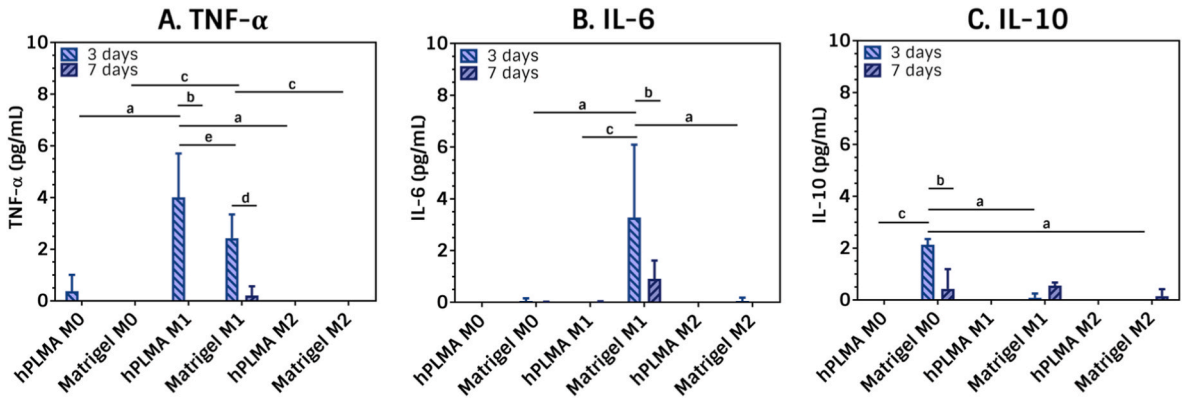

Fig. 5. Expression of TNF-α (**A.**), IL-6 (**B.**), and IL-10 (**C.**) by M0, M1, and M2 macrophages cultured in contact with hPLMA and Matrigel hydrogels. Results are expressed as mean (SD) with n = 3, and with letters (a) to (e) representing significant differences (p-value <0.05).

minimal cytokine induction in macrophages within 3% (w/v) GelMA, failing to elicit significant TNF-α and IL-10 expression after a 48-h culture [45]. Furthermore, in line with our results, in a recent study, Monteiro et al. showed that M0 macrophages cultured in contact with hPLMA hydrogel beads had basal levels of IL-6. However, these macrophages had a high expression of IL-10 and CD36, a marker for the M2 phenotype. This proved that hPLMA hydrogels alone could induce the M2 polarization [20]. Although in our study the IL-10 expression was not detectable in hPLMA conditions, these differences might be related to the specific experimental design used in our work, particularly the intrinsic properties of the hydrogels themselves. Since macrophages were cultured beneath the hydrogels, both hPLMA and Matrigel might have restricted the diffusion of cytokines to the medium. This aligns with findings by Regier et al., who have recently shown that matrix properties, including cytokine sequestration, influence detected cytokine levels in culture media. In their study, out of 21 cytokines analyzed, Matrigel only induced an increase of IL-6 and IL-8 expression in the normal cell lines, yet as mentioned, the Matrigel matrix could have limited the cytokines' diffusion to the medium [46]. Equally, in our work, the low or undetectable cytokine levels in both materials might be explained by the cytokines' retention in the hydrogel's network, rather than their unproduction by the macrophages.

Hence, our results suggest that both hPLMA and Matrigel do not induce exacerbated immune responses and may support both healthy and disease models. As mentioned, despite the consensus of Matrigel immunogenicity, there is insufficient evidence in the literature for this affirmation. In fact, most studies that address this question focus on tumor cell lines and how Matrigel is able to enhance their tumorigenicity [47]. Moreover, it is known that laminin, which is Matrigel's main component, is immunogenic and can interact with different immune cells [48]. Given that the immunogenicity data did not provide robust results, we tried to consolidate these findings by analyzing the transcriptomic profile of hASCs cultured in hPLMA and Matrigel hydrogels.

2.3. *hASCs transcriptomic profile – DEGs functional enrichment*

There are numerous studies assessing the transcriptomic profile of cells encapsulated in Matrigel to study specific cell activities [49–51]. However, the studies evaluating the effect of Matrigel on the cultured cells are much more limited. Most of them focus on the comparison of organoid culture in Matrigel and other matrices, such as decellularized animal-based ECM, hydrogels and composites, but not on the effect of Matrigel on dispersed 3D cell cultures, essential in tissue engineering applications [52,53].

To evaluate the influence of hPLMA and Matrigel on hASCs' behavior at the molecular level, we conducted a total RNA sequencing analysis of hASCs cultured in both materials throughout 0, 1 and 5 days of culture, with day 0 corresponding to the analysis of cells immediately after the cells' encapsulation. Given that Matrigel hydrogels had partial but significant degradation by day 7, the analysis was limited to 5 days of culture to ensure the integrity of the Matrigel matrix. A similar analysis, to critically compare the effects of these 3D matrices with traditional 2D culture, was performed. To do that, the RNA profiles of hASCs cultured in 2D were analyzed at day 0 and compared with those of 3D encapsulated cells in hPLMA and Matrigel. This analysis revealed 20,809 expressed genes. Thus, to refine the analysis and focus on biologically meaningful changes, we applied strengthened selection criteria: an adjusted p-value <0.01, a false-discovery rate (FDR) p-value <0.05, and an absolute fold change >2. Using these thresholds, we identified 701 differentially expressed genes (DEGs) between 2D and hPLMA (Figure S.1), and 2081 DEGs between 2D and Matrigel, of which 466 were common to both groups. The principal component analysis (PCA) plot (Fig. 6) illustrated a clear separation in gene expression profiles among the different culture conditions, i.e., hASCs cultured in 2D, hPLMA and Matrigel, with 58% variance in the first principal component (PC). The second PC, with 20% variance, separated the days of culture, while the third PC had the smallest variance (10%) and represented the different assays conducted. This indicates that, despite the effective hASCs growth in each matrix, their molecular behavior is considerably different in each material and also varies throughout the culture time. Likewise, the volcano plots (Figure S.2) demonstrate a higher dispersion of DEGs in hASCs cultured in Matrigel, compared to those in hPLMA. This shows that the DEGs of hASCs in Matrigel generally have higher fold changes and more statistically significant differences in gene expression. Despite this difference in the number of DEGs, the changes in gene expression alone do not provide a complete overview of the cell state unless it is known the biological pathways in which these genes are involved. Therefore, we further analyzed the processes associated with these DEGs to better understand how the transcriptional changes translate into cell responses in each condition.

Considering the top 20 DEGs with the highest absolute fold changes across the different conditions (Figure S.3), the G:Profiler tool was used to investigate the corresponding gene ontology (GO) terms enriched for these DEGs, i.e., it was used to investigate which biological processes, cellular components, or molecular functions were most affected in our dataset, providing insight into the functional implications of the observed gene expression changes. The corresponding results are summarized in Table S.2. Notably, the most upregulated DEGs from day 0, that is, immediately after encapsulation, revealed distinct molecular patterns between the two matrices, even though they have no enrichment for specific cellular functions, particularly within the Matrigel matrix. In hPLMA, the top DEGs were primarily enriched in processes related to protein folding, responses to abiotic stimuli, and the regulation of cell proliferation and apoptosis, largely linked to the nucleus and cytoskeleton. Likewise, at day 1, the top DEGs of hASCs in hPLMA hydrogels continued to be mostly associated with RNA processing and

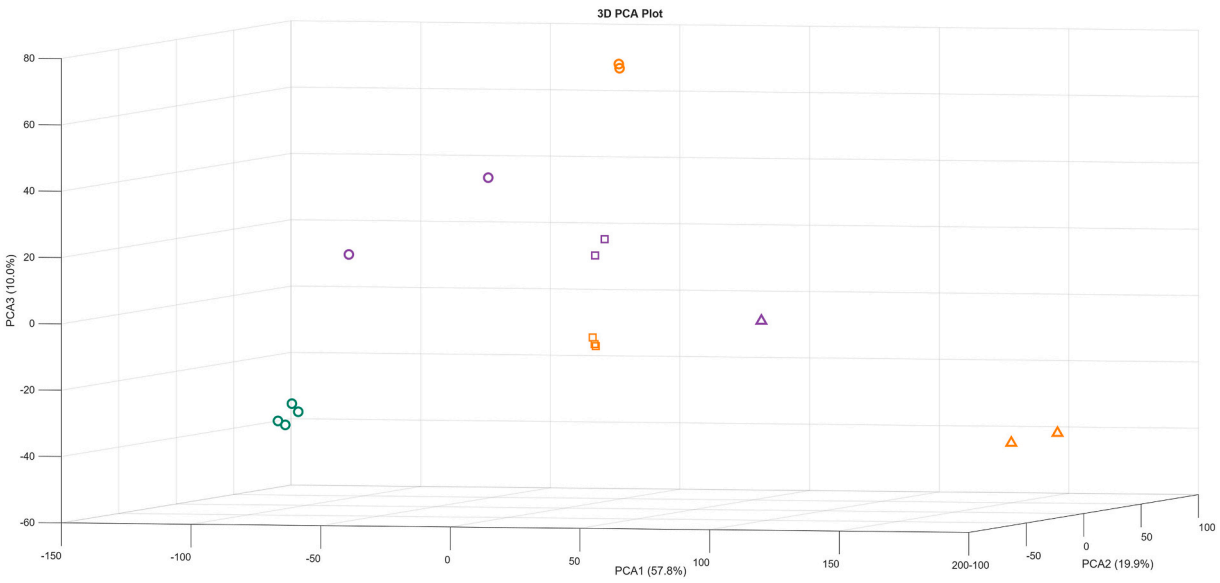

Fig. 6. PCA analysis of genes expressed in hASCs cultured in 2D, and hPLMA and Matrigel hydrogels.

oxidoreductase activity. Conversely, the Matrigel-cultured cells top DEGs were enriched in differentiation-related processes, the leptin and the Wnt pathways, as well as response to oxygen-containing compounds and endogenous stimuli. After 5 days, hASCs embedded in hPLMA maintained enrichment in RNA and DNA processing, regulation of cellular processes, tissue development, and response to lipids, oxygen-containing compounds and tumor necrosis factor. Conversely, the top DEGs in the Matrigel condition increasingly reflected cytokine and chemokine activities, inflammatory and defense responses, and chemotaxis while still showing enrichment for responses to lipids,

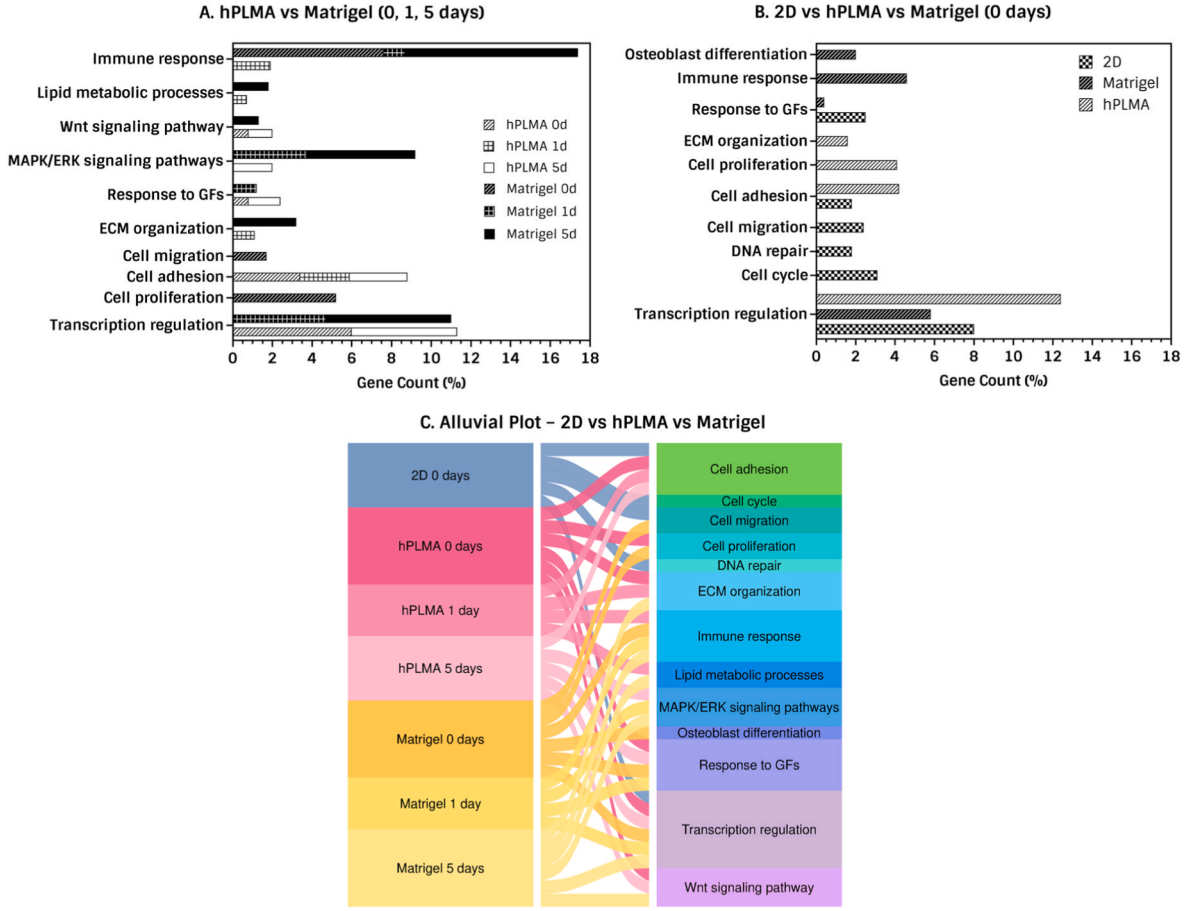

Fig. 7. Main clusters of biological processes enriched in DEGs between hPLMA and Matrigel at 0, 1 and 5 days of culture (**A.**), and between 2D, hPLMA, and Matrigel at 0 days of culture (**B.**). Results are shown as the percentage of DEGs in each category. (**C.**) Alluvial plot of 2D, hPLMA and Matrigel conditions (left) and biological processes (right) with the edge representing the relationship between them.

oxygen-containing compounds and chemical stimuli. Collectively, these findings suggest that biochemical composition and/or mechanical properties of Matrigel may elicit defense or immune-related responses from the encapsulated cells, as several of the most upregulated genes are linked to immune functions.

To have a deeper understanding of the cellular processes influenced by each material over different time points, and since the most upregulated DEGs do not represent the whole cell state, all the DEGs for each condition were analyzed using the DAVID Bioinformatics' Functional Clustering tool. This tool helped the identification of enriched GO terms and subsequently organized these terms into clusters of gene functions. To simplify this analysis, we grouped the clusters with similar terms into broader categories. As a result, Fig. 7A shows the main cluster categories comparing hPLMA and Matrigel at 0, 1 and 5 days of culture, and Fig. 7B presents the main cluster categories comparing 2D culture with hPLMA and Matrigel at day 0. The alluvial plot (Fig. 7C) visually represents the associations between each condition and the corresponding biological processes.

At day 0, the DEGs in the hPLMA condition indicate an early modulation of genes involved in transcriptional regulation, cell adhesion, and response to GFs. This pattern persisted at day 1, with the additional enrichment for ECM organization processes, suggesting that cells begin to adapt and reorganize the hPLMA matrix shortly after the encapsulation in this material. Immune-related processes were also enriched at this time point, which may reflect the cellular adaptation to this new environment. However, by day 5, these processes were no longer enriched among hASCs in hPLMA, which shows that this was likely a transitory adaptation of the cells to the new material and not an exacerbated and chronic response that would be indicative of material immunogenicity. Notably, at day 5, there was still enrichment for cell adhesion, ECM organization, transcription regulation, and response to GFs, confirming that, since the encapsulation, hASCs can adhere, proliferate and organize the hPLMA matrix. Additionally, the continuous response to GFs can likely be attributed to the sustained release of these factors from the hPLMA matrix, as demonstrated in previous research [37].

In contrast, Matrigel maintained a consistent enrichment for immune response processes from day 0 to day 5, indicating that it induces a constant defense state in the cells. Throughout the period of the assay, there was also enrichment in processes related to cell migration, proliferation, transcription regulation, and response to GFs, an expected outcome given the broad range of GFs inherently present in Matrigel [54]. Additionally, genes involved in lipid metabolism were enriched in cells cultured in both hPLMA and Matrigel. This enrichment likely reflects the intrinsic hASCs activity in regulating lipid metabolism in the organism [55].

When comparing hASCs cultured in 3D environments to those maintained in 2D conditions, it was noticeable that the hPLMA condition had more enrichment for cell adhesion and proliferation, transcription regulation, and ECM organization. These results highlight hPLMA's capacity to recapitulate key features of the native cellular microenvironment, thereby supporting cell growth and migration within a 3D context. This also indicates that the cell encapsulation in hPLMA hydrogels, including exposure to a photoinitiator and light, did not exert significant detrimental effects on the cells. Conversely, hASCs embedded in Matrigel had greater enrichment in immune response processes, differentiation, and transcriptional regulation genes when compared to both 2D and hPLMA-encapsulated cells.

2.4. hASCs transcriptomic profile – in-depth DEGs analysis

2.4.1. Immunomodulation and matrix-driven transcriptional programming in hPLMA vs. Matrigel

Considering the main cell functions that were enriched for each condition, we conducted an in-depth analysis of DEGs involved in specific hASCs activities, focusing on six key cellular functions: hASCs immunomodulation; differentiation; proliferation; angiogenesis and response to hypoxia; cell-cell and cell-ECM adhesion; ECM remodeling and mechanotransduction.

When introduced into the human body, hASCs have the ability to evade immune recognition, resulting in low immunogenicity and making them suitable candidates for stem cell therapies [56]. Thus, when embedded in hydrogels that accurately replicate the human ECM, hASCs should exhibit this immunomodulatory effect and reduce the release of inflammatory cytokines. To thoroughly delineate the immunomodulatory landscape and matrix-dependent cellular responses, we examined pivotal DEGs at early (day 0), intermediate (day 1), and later (day 5) time points. This temporal analysis demonstrated a gradual divergence between hPLMA and Matrigel, encompassing inflammatory signaling, matrix remodeling, and tissue maturation. At baseline (day 0), hASCs displayed distinct transcriptional profiles depending on the culture condition, indicating an immediate response to both dimensionality and matrix composition. Regarding immunomodulation (Fig. 8A), it is evident that hASCs cultured in both hPLMA and Matrigel expressed factors typically produced by mesenchymal stem cells (MSCs) when grown in 3D cultures, such as *TNFAIP6* and *IL24*. Particularly, *IL24* had a significantly higher expression in Matrigel compared to hPLMA cultures. This higher *IL24* expression may act as a compensatory mechanism to counteract the significant pro-inflammatory profile in Matrigel. Indeed, Matrigel induced a prolonged pro-inflammatory state, characterized by continuous upregulation of key cytokines and chemokines such as *IL6, IL1B, IL8, CCL2*, and *CXCL2*, indicating chronic activation of innate immune pathways and a chemokine-driven inflammatory niche [57]. Early activation of innate immune pathways was accompanied by elevated *ICAM1* expression (Fig. 8D), indicating enhanced adhesive and immune-interactive properties. In contrast, hPLMA supported a transient immune response that resolved over time, promoting the production of immunoregulatory mediators such as *TNFAIP6* and *CD200*, both associated with anti-inflammatory signaling and immune suppression, along with *PTGER2*, indicating activation of prostaglandin-mediated immunomodulation. This suggests that hASCs embedded in Matrigel maintain a constant expression of pro-inflammatory genes that surpasses those in hPLMA hydrogels. The plots from the DICE tool also illustrate how immune activation profiles change over time (Fig. 9). As shown in Fig. 9A, the enrichment of pro-inflammatory genes (*IL1B, IL8, CCL2, CXCL2*) in Matrigel is associated with monocyte/macrophage and neutrophil profiles, which indicates immediate activation of innate immune pathways. At day 5 (Fig. 9C), Matrigel continues to have high expression of immune-related genes, associated with ongoing matrix degradation (*MMP3, MMP9*) and monocyte/macrophage profiles. Dessels et al. have shown that hASCs supplementation with FBS enriches immune response and differentiation processes. However, in this study, as both cultures had FBS supplementation, we can attribute the constant enrichment in immune processes solely to Matrigel [58]. It is also worth noting that previous proteome array analysis of Matrigel identified relatively high levels of several chemokines in this matrix, such as CXCL9, PAI-1, CCL2, and CCL12 [59]. The presence of these molecules in Matrigel, even in small amounts, can likely trigger pro-inflammatory cellular responses.

Previous studies indicate that the expansion of hASCs does not diminish their immunomodulatory properties until passage 6 [60,61]. In this analysis, we identified a single marker of the hASCs' immunosuppressive effect, *CD200*, which was upregulated in both Matrigel and hPLMA, indicating that the hASCs used in this assay were producing immunoregulatory markers. Although it was not possible to identify *IDO* or *PGE2* in the DEGs, both immunomodulation markers, we identified the expression of prostaglandin E2 receptor gene, *PTGER2*, corroborating hASCs' immunosuppressive function [56]. Particularly, *PTGER2* expression was higher in both Matrigel and hPLMA compared to the 2D culture (Fig. 8D), confirming that 3D matrices are more conducive to hASCs' immunomodulation function, as shown in previous studies [56].

When embedded in a 3D matrix, cells experience restricted nutrient

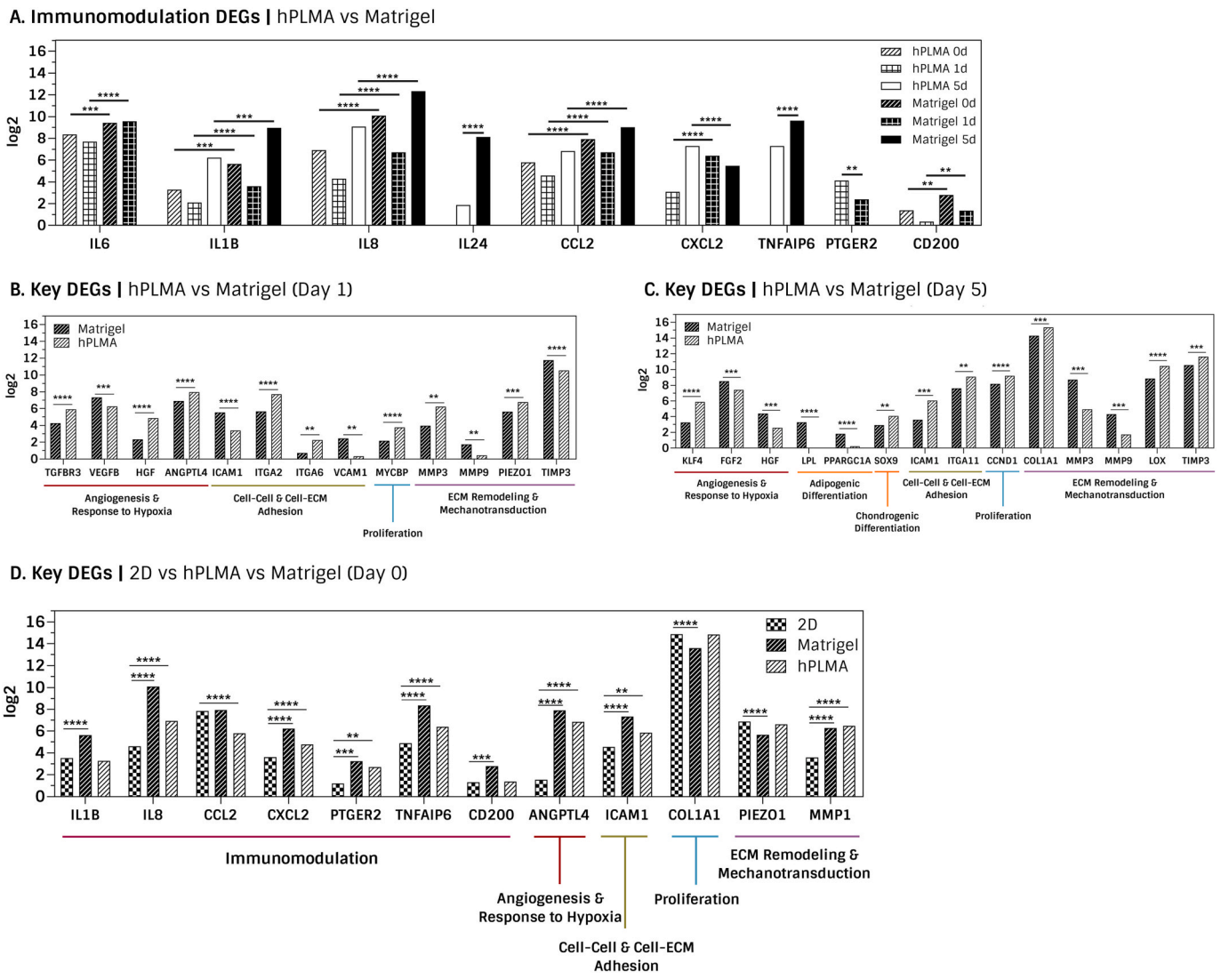

Fig. 8. Absolute log2 fold change of key DEGs involved in hASCs' immunomodulation (**A.**) and other hASCs' functions (angiogenesis and hypoxia; differentiation; cell adhesion; proliferation and ECM remodeling) (**B.** and **C.**), for hASCs cultured in hPLMA and Matrigel hydrogels, for 0, 1, and 5 days of culture. Absolute log2 fold change of key DEGs involved in hASCs' immunomodulation; angiogenesis and hypoxia; cell adhesion; proliferation and ECM remodeling, for hASCs cultured in 2D, hPLMA hydrogels and Matrigel hydrogels for 0 days of culture. (**D.**) ** p-value <0.01, *** p-value <0.001 and **** p-value <0.0001.

and gas exchanges, which naturally stimulates the expression of hypoxia and angiogenesis markers, as the lack of oxygen promotes capillary formation [62]. Although specific DEGs for hypoxia markers were not identified, both materials induced the expression of angiogenic markers, which are often linked to hypoxic conditions (Fig. 8B and C). Genes related to angiogenesis and trophic support were upregulated in both matrices. Particularly, hASCs in hPLMA presented higher expression of *TGFBR3*, *HGF*, and *ANGPTL4* at day 1, and *KLF4* at day 5. In contrast, hASCs within Matrigel showed an increased expression of *VEGFB* at day 1, and *FGF2* and *HGF* at day 5. The upregulation of these genes is likely linked to the presence of GFs that promote angiogenesis, such as VEGF, PDGF and fibroblast growth factor (FGF), in both matrices, and indicates activation of pathways that promote tissue repair [62]. Together with the previous viability results, we conclude that the cells were not in a state of severe hypoxia. However, this restricted 3D environment, especially in the Matrigel aggregates at day 7, appears to have triggered angiogenic pathways to improve the cells' nutrient and gas exchanges.

Regarding differentiation markers, we identified triggers of adipogenic differentiation, particularly *LPL* and *PPARGC1A*, exclusively in Matrigel hydrogels at day 5 (Fig. 8C) [63]. Previous research by Kim et al. indicated that *PPARγ*, an early adipogenic marker, exhibited higher expression levels in softer GelMA matrices, with this expression decreasing as the hydrogel stiffness increased [64]. Similarly, Matrigel being considerably softer than hPLMA provides a more permissive microenvironment for adipogenic differentiation, which may explain the enhanced expression of adipogenic markers observed in this condition. Even so, previous studies have shown that hASCs differentiation is generally accompanied by a reduction in proliferative activity, as cells transition from growth toward lineage-specific specialization [65]. However, in the present study, the encapsulated hASCs maintained high proliferation rates throughout the culture period, suggesting that they did not enter a differentiation program but instead remained metabolically active and proliferative. This behavior likely results from the intrinsic properties of the 3D matrices. In particular, the presence of angiogenic and mitogenic GFs, such as VEGF, PDGF, and FGF, within these hydrogels may further support proliferation and metabolic activity [66]. Additionally, the culture duration might not have been sufficient to induce terminal differentiation, particularly in the absence of defined differentiation stimuli [67]. In hPLMA, only *SOX9*, a known chondrogenic differentiation marker, was expressed, also suggesting an inert behavior towards differentiation.

In both materials, hASCs showed high expression of cell adhesion

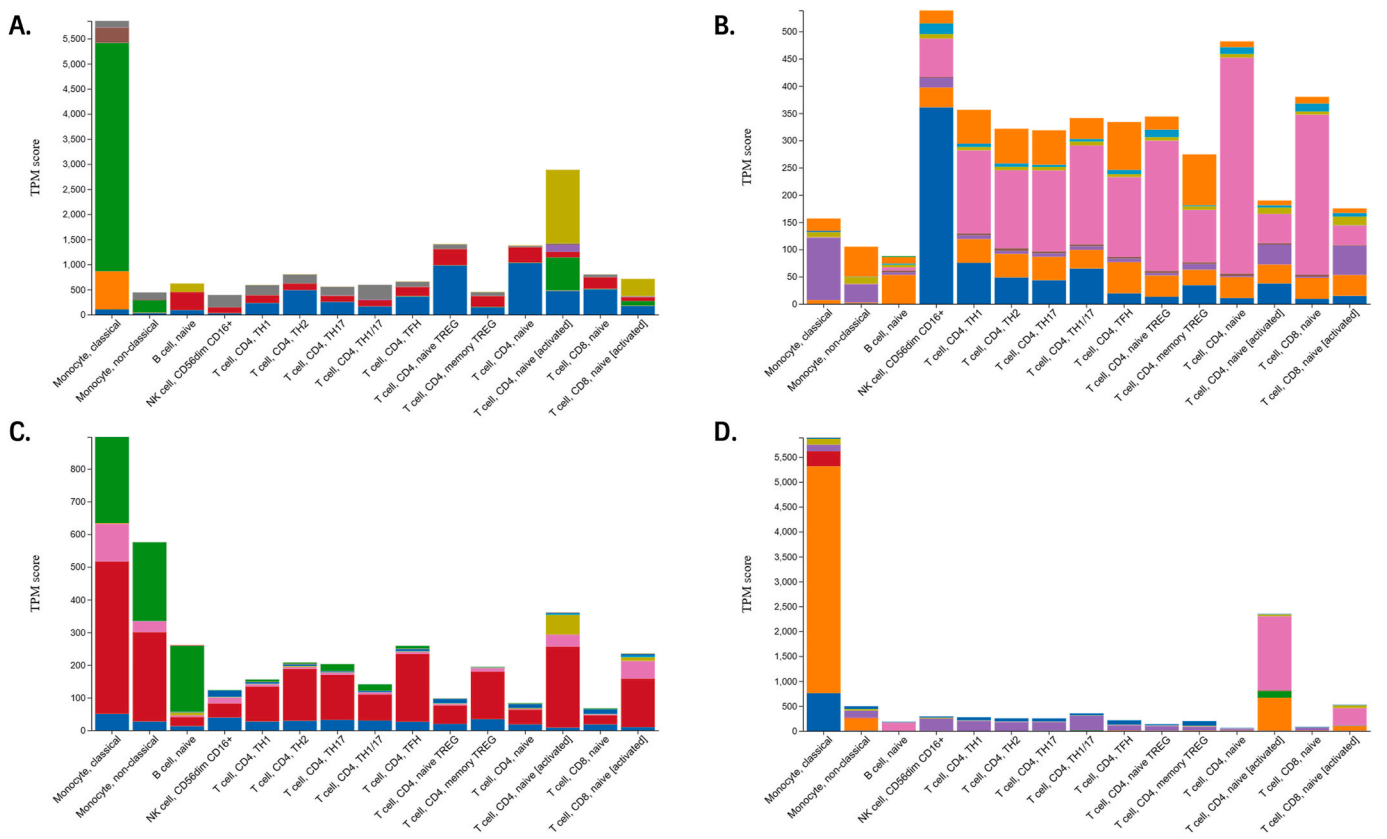

Fig. 9. Matrix-dependent immunomodulation and temporal transcriptional dynamics of hASCs in 2D, Matrigel, and hPLMA. (**A–D**) Stacked bar plots display the TPM scores of selected DEGs across various immune cell types, as inferred by the DICE tool. (**A**) Baseline (Day 0: 2D vs. Matrigel vs. hPLMA). (**B**) Initial reaction (Day 1: hPLMA vs. Matrigel). (**C**) Later response (Day 5: hPLMA vs. Matrigel). (**D**) Immune system changes over time (0–5 days). Matrigel demonstrates a continuous increase in pro-inflammatory cytokines and chemokines (*IL6, IL1B, IL8, CCL2, CXCL2*) at all time points, indicating persistent activation of innate immune pathways. hPLMA elicits a transient immune response during the initial stages (day 0–1), resolving by day 5, as shown by increased expression of immunoregulatory mediators (*TNFAIP6, CD200*).The inputted genes for each plot are presented in Table S.3.

markers, such as *ITGA2*, *ITGA6*, *ICAM1,* and *VCAM1* at day 1, as well as *ICAM1* and *ITGA11* at day 5, indicating the formation of cell-matrix interfaces. These markers encode for adhesion proteins, primarily involved in integrin-mediated adhesion [68,69]. Interestingly, Ren et al. reported that ICAM-1 and VCAM-1 are also involved in MSCs immunomodulation, as they are crucial for the adhesion of stem cells and immune cells [70]. Therefore, this confirms that hASCs were maintaining their immunosuppressive function. Additionally, hPLMA-encapsulated cells demonstrated higher expression of proliferation markers, including *MYCBP* and *CCND1*, both involved in the regulation of transcription and cell cycle progression, which was expected since transcription regulation processes were constantly enriched for the hPLMA conditions [71,72].

As previously discussed, hASCs secrete several MMPs, particularly collagenases, to remodel the surrounding matrix [34]. Here, we found a high expression of *MMP3* and *MMP9* in Matrigel conditions, particularly at day 5, indicating active and unresolved proteolytic processes, and persistent matrix remodeling. This is also consistent with the predominance of collagen IV in the Matrigel matrix. Additionally, the expression of MMPs inhibitors, the TIMPs, such as *TIMP3*, suggests a balanced synthesis of MMPs necessary for matrix remodeling in both hPLMA and Matrigel hydrogels. However, in Matrigel, the presence of *TIMP3* appeared insufficient to prevent degradation. It should be noted that Matrigel inherently contains MMPs and TIMPs, which could have influenced the production of these molecules by hASCs [35]. In contrast, hPLMA had a higher expression of *PIEZO1*, a mechanotransduction gene [73]. Together with the proliferation markers *MYCBP* and *CCND1*, this demonstrates that hASCs could perceive hPLMA and remodel this matrix accordingly. By day 5, hPLMA promoted a transcriptional program consistent with tissue maturation and structural stabilization, as shown by increased *COL1A1* and *LOX* expression, markers of collagen deposition and crosslinking, respectively [74]. Upregulation of *ITGA11* further supported enhanced cell-matrix interactions, while transcriptional regulators such as *KLF4*, *PPARGC1A*, and *SOX9* indicated ongoing cellular adaptation. It is also worth noting that several of these ECM remodeling markers, including MMP-3, MMP-9, and immunomodulation markers, such as CCL2, CXCL2 and IL-1β are actively involved in angiogenesis regulation, showing the interconnected nature of these biological processes [75].

Collectively, these findings indicate that hPLMA provides a more regulated, immunologically balanced, and tissue-mimetic microenvironment, facilitating ECM organization, mechanosensitive adaptation, and resolution of initial immune responses. In contrast, Matrigel induces a persistent inflammatory and proteolytic state that impedes the formation of stable tissue architecture over time.

2.4.2. SIGNOR network analysis of signaling programs in hPLMA and Matrigel

To better understand the signaling mechanisms underlying the observed transcriptional differences, we used the SIGNOR database for pathway and causal network analysis. This approach enabled the identification of key regulatory interactions linking DEGs to functional signaling pathways under different culture conditions and at various time points.

SIGNOR analysis (Fig. 10) revealed that the signaling network architectures of hPLMA and Matrigel were markedly different. Under

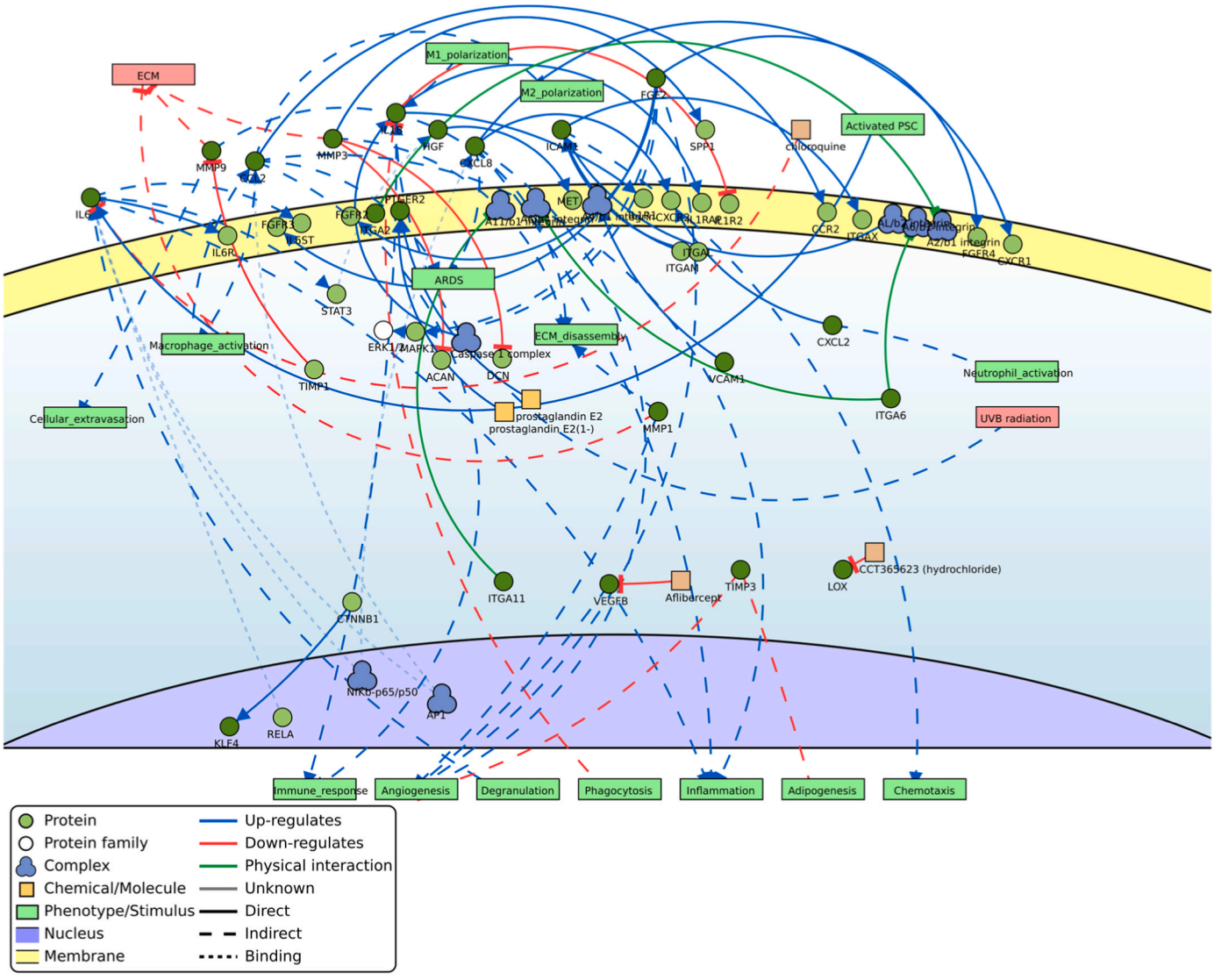

Fig. 10. SIGNOR-based network analysis illustrating key signaling interactions derived from DEGs in hASCs cultured in hPLMA and Matrigel. Matrigel conditions show enrichment of pro-inflammatory signaling hubs, including IL-1, TNF, and NF-κB pathways, forming highly interconnected networks associated with sustained immune activation. In contrast, hPLMA displays a more balanced network, with increased representation of immunoregulatory (*TNFAIP6, PTGER2*) and mechanotransduction-related (*PIEZO1*) pathways, indicating controlled immune modulation and matrix adaptation. Overall, the networks highlight a pro-inflammatory signaling dominance in Matrigel vs. a regulated, tissue-supportive signaling profile in hPLMA.

Matrigel conditions, the network was dominated by pro-inflammatory signaling hubs, with significant activation of pathways associated with the NF-κB, IL-1, and TNF signaling axes. *IL1B*, *IL6*, and *CXCL8* (IL8) served as central nodes and upstream regulators, increasing the expression of chemokines (*CCL2*, *CXCL2*) and amplifying inflammatory cascades. These interactions formed a highly interconnected network, characteristic of sustained innate immune responses. The persistence of these signaling relationships over time suggests that Matrigel maintains a stable pro-inflammatory feedback loop, supporting the "alert" state observed in the DEGs analysis. In contrast, hPLMA exhibited a more balanced and modular signaling network, characterized by the presence of both immunoregulatory and tissue-repair pathways. Key nodes such as *TNFAIP6* and *PTGER2* were associated with inhibitory edges targeting inflammatory mediators, indicating active suppression of excessive immune activation. The hPLMA network contained fewer pro-inflammatory feedback loops and more compartmentalized pathways compared to the dense inflammatory network in Matrigel.

Additionally, signaling pathways related to mechanotransduction and the ECM were organized differently in each condition. In hPLMA, *PIEZO1*-associated signaling integrated mechanical sensing with downstream regulatory pathways, potentially linking matrix stiffness to regulated cellular adaptation. Both conditions featured ECM remodeling nodes, such as MMPs and *TIMP3*, but their roles differed. Matrigel networks favored activation of proteolytic activity, while hPLMA networks favored its inhibition, suggesting tighter control of matrix turnover in hPLMA.

Temporal network analysis further showed that, while Matrigel sustained consistent activation of inflammatory signaling hubs from day 0 to day 5, hPLMA networks shifted toward reduced connectivity of inflammatory nodes and increased prominence of regulatory and structural pathways. By day 5, hPLMA networks displayed abundant interactions related to ECM organization, differentiation, and metabolic adaptation, whereas Matrigel maintained dense inflammatory and degradative signaling frameworks. Thus, SIGNOR-based network analysis supports the conclusion that Matrigel drives a self-sustaining pro-inflammatory signaling network, while hPLMA fosters a controlled signaling environment that integrates immune modulation, mechanotransduction, and tissue maturation. These findings enhance our

understanding of how matrix composition influences not only gene expression but also the signaling logic governing cellular behavior.

Collectively, the transcriptomic data consolidate our previous results, demonstrating that, equally to Matrigel, hPLMA hydrogels allow cell-cell and cell-ECM adhesion, and the ECM remodeling, which allows their migration, proliferation and perception of the matrix. However, despite the cells appearing to have normal growth at the macromolecular level, Matrigel consistently induced significantly higher expression of immune-related genes since the encapsulation. Even though Matrigel did not enable cell culture for long periods, it would be relevant to analyze processes at the genomic level, such as differentiation, to understand how hPLMA hydrogels influence the cells during long-term cultures.

Although one of our aims is to move towards xeno-free and human-based 3D cell cultures, we maintained FBS supplementation in this study to allow better comparison with the bulk of the literature on this topic. Hence, for future studies, it would be relevant to replace FBS with human-based supplementation, such as hPL. Particularly, in hASCs culture, hPL showed to improve cell proliferation without inducing cell differentiation and immune responses, unlike FBS [58]. This would allow us to understand and confirm if FBS has any major influence on the cell's response to the matrix, especially at the molecular level. Ultimately, this study provides a multi-layered characterization of how matrix origin and composition shape cellular behavior in 3D culture systems, integrating phenotypic, transcriptomic, and network-level analyses. While both hPLMA and Matrigel supported hASCs' viability and proliferation, our data reveal a fundamental divergence in the biological programs they induce. Specifically, Matrigel promotes a persistent inflammatory and proteolytic state, whereas hPLMA supports a regulated, immunomodulatory, and tissue-mimetic microenvironment. This distinction was consistently observed across DEGs profiling, functional enrichment, immune inference (DICE), and causal signaling networks (SIGNOR), indicating that matrix composition governs not only gene expression but also the underlying signaling logic of cell adaptation.

3. Conclusion

The present study demonstrated the differences in cell behavior when encapsulated in hPLMA and Matrigel hydrogels. At a macromolecular level, both matrices supported regular cell growth and proliferation with increasing metabolic activity. However, Matrigel's soft nature led to rapid degradation and the formation of large clusters of cells. This work also represents the first immunological and transcriptomic analysis of hPLMA hydrogels and their direct comparison with Matrigel. Although cytokine quantification on macrophage cultures showed basal expression of both pro- and anti-inflammatory markers, the transcriptomic analysis showed that Matrigel consistently induced a higher expression of immune-related genes in hASCs compared to hPLMA. Moreover, the transcriptomic data corroborated our previous findings demonstrating that hASCs in hPLMA hydrogels had greater enrichment for regulatory cellular processes, with lower expression of immune or differentiation pathways. Ultimately, these findings confirm our initial hypothesis, demonstrating that hPLMA effectively mimics the human ECM, supporting prolonged culture while maintaining matrix stability, high cell viability, and sustained cell proliferation. Collectively, the results position hPLMA hydrogels as a robust and reproducible human-derived alternative to Matrigel, offering a more defined, stable, and ethically sustainable platform for next-generation 3D cell culture and tissue engineering applications.

4. Methods

In vitro Cell Culture – hASCs culture: Human adipose-derived stem cells (hASCs) were obtained from subcutaneous adipose tissue at Hospital da Luz (Aveiro, Portugal), with informed patient consent. The cells were then isolated from the tissue, following the protocol described by Correia et al. [76] The cells were cultured in Minimum Essential Medium Alpha (α-MEM, Gibco™, Thermo Fisher Scientific Inc., USA), supplemented with 10% (v/v) heat-inactivated FBS (Gibco™, Thermo Fisher Scientific Inc., USA), 1% (v/v) antibiotic/antimycotic (Gibco™, Thermo Fisher Scientific Inc., USA) and $NaHCO_3$ (Sigma-Aldrich®, USA). The hASCs were used between passages 2 and 8.

In vitro Cell Culture – hASCs encapsulation in hPLMA and Matrigel Hydrogels: For encapsulation in hPLMA and Matrigel hydrogels, hASCs were trypsinized (trypsin/EDTA solution, Gibco™, Thermo Fisher Scientific Inc., USA) and then incorporated into the hPLMA solution at a density of 3×10^6 cells mL^{-1} or the Matrigel solution with a density of 2×10^6 cells mL^{-1}. hPLMA hydrogels were synthesized according to the manufacturer's instructions. Briefly, 50 μL/well of a 15% (w/v) hPLMA (Metatissue®, Portugal) solution with 0.5% (w/v) solution of lithium phenyl-2,4,6-trimethylbenzoylphosphinate (LAP, Metatissue®, Portugal) in phosphate-buffered saline (PBS, Sigma-Aldrich®, USA) was pipetted to a 96-well plate. Each well was irradiated with a 405 nm LED curing light (Valo™ Cordless, Ultradent Products Inc., USA) for 60 s to synthesize the hydrogels. Matrigel hydrogels were synthesized according to the manufacturer's instructions. After Matrigel's thawing, 50 μL/well of a 1.2% (w/v) Matrigel (Corning®, USA) solution was pipetted to a 96-well plate. The solution was incubated for 60 min at 37°C with 5% CO_2 to polymerize the matrix and create hydrogels. To assess batch-to-batch consistency, three independent batches of both hPLMA and Matrigel were purchased and evaluated regarding cell metabolic activity and cell viability.

Biological Characterization – Cell Metabolic Activity Quantification: The Cell Counting Kit-8 assay (CCK-8, MCE®, USA) was applied to quantify hASCs' metabolic activity. At each time point, namely 0, 1, 3, 7 and 14 days of culture, 10 μL/well of the CCK-8 reagent solution and 100 μL/well of FBS-depleted α-MEM medium were added to a 96-well plate, and it was incubated for 4 h at 37°C with 5% CO_2. Then, the absorbance (ABS) was read at 450 nm using the SpectraMax iD3 Microplate Reader (Molecular Devices, USA). This assay used five replicates of cell-loaded hPLMA and Matrigel hydrogels for each time point.

Biological Characterization – Cell Viability by Live/Dead assay: The hASCs' viability was assessed using two fluorescent probes, specifically calcein acetoxymethyl (calcein AM) and propidium iodide (PI) to identify live and dead cells, respectively. At each time point, i.e., 1, 3 and 7 days of culture, the cell-laden hydrogels were washed with PBS and incubated for 30 min at 37°C with 5% CO_2, in a solution with 1:1000 of PI (Invitrogen™, Thermo Fisher Scientific Inc., USA), and 1:500 of calcein AM (Invitrogen™, Thermo Fisher Scientific Inc., USA) diluted in PBS. The hydrogels were then washed with PBS and visualized under a fluorescence microscope (Thunder, Leica, Germany). The images were processed using the LAS X Software (Leica, Germany).

Biological Characterization – Cell Proliferation by Ki-67 staining: The Kiel 67 (Ki-67) antigen was used to quantify the hASCs' proliferation, since Ki-67 expression increases solely during the active cell cycle. At each time point (0, 3 and 7 days of culture), the cell-laden hydrogels were washed with PBS and fixed with a 4% (v/v) paraformaldehyde (PFA, Thermo Fisher Scientific Inc., USA) solution for 1 h (hPLMA hydrogels) or 30 min (Matrigel hydrogels). The Ki-67 immunostaining was carried out using the CytoVista™ Tissue Clearing/Staining Kit (Invitrogen™, Thermo Fisher Scientific Inc., USA), according to the manufacturer's instructions. Briefly, the hydrogels were incubated overnight at 4°C with the primary antibody, Ki-67 Recombinant Rabbit Monoclonal Antibody (Invitrogen™, Thermo Fisher Scientific Inc., USA) at 2.5 μg mL^{-1}. The following day, they were incubated for 3 h with a detection antibody, namely the Goat anti-Rabbit IgG (H + L) Highly Cross-Adsorbed Secondary Antibody, Alexa Fluor™ Plus 488 (Invitrogen™, Thermo Fisher Scientific Inc., USA) at 4 μg mL^{-1}. After washing with PBS, the hydrogels were examined under a fluorescence microscope. The Ki-67 expression was quantified using the ImageJ software (version 1.54j, National Institutes of Health, USA). For this, the fluorescence intensity of regions with Ki-67 expression was measured,

and the background signal was excluded based on the corrected total cell fluorescence (CTCF) equation (**Equation I**) [77]. At each condition, the average CTCF of 100 regions of interest (ROI) of Ki-67 expression was used to determine the fold change in Ki-67 expression compared to day 0.

$$CTCF = Integrated\ Density - (Area\ of\ Selected\ Cell \times Average\ Mean\ Gray\ Value\ of\ Background)$$

Equation I. The corrected total cell fluorescence (CTCF) is obtained with the "Integrated Density" as the mean gray value, i.e., the mean of pixels in a section of the image, multiplied by the area of Ki-67 expression. The "Area of Selected Cell" represents the ROI of Ki-67 expression, and the "Average Mean Gray Value of Background" is the average of pixels in regions with background signal.

Biological Characterization – Cell Morphology Analysis: To assess how the hPLMA and Matrigel hydrogels influence hASCs' morphology, two fluorescent stains were used, specifically 4′,6-diamidino-2-phenylindole (DAPI) and phalloidin, which stain cell nuclei and actin filaments, respectively. At three selected time points, namely 0, 3 and 7 days of culture, cell-laden hPLMA and Matrigel hydrogels were washed with PBS and fixed with a 4% (v/v) PFA solution as described. For the phalloidin staining, the hydrogels were incubated for 45 min at RT with a 1:400 rhodamine-phalloidin (Thermo Fisher Scientific Inc., USA) solution diluted in PBS. After washing with PBS, the hydrogels were incubated for 5 min at RT with a 1:1000 DAPI (Thermo Fisher Scientific Inc., USA) solution diluted in PBS. The hydrogels were washed with PBS, and cell morphology was analyzed under a fluorescence microscope.

Immunogenicity Evaluation – Cell Culture, Differentiation and Polarization: The THP-1 cell line was used to assess the immunogenic profile of hPLMA and Matrigel hydrogels, since these cells can be differentiated into different types of macrophages. THP-1 cells were kindly provided by Professor João Mano from the University of Aveiro. The cells were cultured in single cell suspension, with Roswell Park Memorial Institute Medium (RPMI) 1640 (Sigma-Aldrich®, USA) supplemented with N′-2-Hydroxyethylpiperazine-N′-2-ethane sulphonic acid (HEPES, Sigma-Aldrich®, USA), 1% (v/v) sodium pyruvate (Lonza, Switzerland), 1% (v/v) antibiotic/antimycotic (Gibco™, Thermo Fisher Scientific Inc., USA), 10% (v/v) heat-inactivated FBS (Gibco™, Thermo Fisher Scientific Inc., USA), and $NaHCO_3$ (Sigma-Aldrich®, USA).

The THP-1 monocytes were chemically differentiated into monocyte-derived macrophages (M0 macrophages) and polarized into classically activated M1 macrophages and alternatively activated M2 macrophages, based on the method described by Genin et al. [78] THP-1 cells (5×10^6 cells mL^{-1}) were cultured in 96-well plates for 24 h with RPMI 1640 medium supplemented with 50 ng mL^{-1} of phorbol 12-myristate 13-acetate (PMA, MCE®, USA), followed by a 24-h incubation with RPMI 1640 medium. Afterwards, M0 macrophages were polarized into M1 macrophages with a 48-h incubation with a co-culture medium of α-MEM and RPMI 1640 media (at a 1:1 ratio), supplemented with LPS (MCE®, USA) at 10 ng mL^{-1} and INF-γ (MCE®, USA) at 40 ng mL^{-1}. The polarization into M2 macrophages required a 48-h incubation of a co-culture medium of α-MEM and RPMI 1640 media (at a 1:1 ratio), supplemented with IL-4 (MCE®, USA) at 40 ng mL^{-1} and IL-13 (MCE®, USA) at 40 ng mL^{-1}. Finally, ⌀ 6 mm hPLMA hydrogels at 15% (w/v) and Matrigel hydrogels at 1.2% (w/v) were synthesized on top of the macrophages as previously described. Then, the medium of each type of macrophage was collected at 3 and 7 days of culture.

Immunogenicity Evaluation – Immunological Assays: To identify the activation of an immune response, the concentration of three types of cytokines, namely tumor necrosis factor-alpha (TNF-α), interleukin-6 (IL-6), and interleukin-10 (IL-10), were quantified using ELISA kits. TNF-α and IL-6, both pro-inflammatory cytokines, were selected to evaluate M1 macrophages' activity. IL-10, an anti-inflammatory cytokine, was used to assess the activity of M2 macrophages. Each ELISA kit (Invitrogen™, Thermo Fisher Scientific Inc., USA) was performed following the manufacturer's instructions. The absorbance was read using the SpectraMax iD3 Microplate Reader.

Transcriptomic Profile – RNA purification and quantification: hASCs below passage 6 were cultured in 15% (w/v) hPLMA hydrogels and 1.2% (w/v) Matrigel hydrogels for 5 days, as previously described. At specific time points (0, 1 and 5 days of culture), hASCs were recovered from hPLMA hydrogels through enzymatic digestion of the hydrogels. Matrigel hydrogels were dissolved using TRIzol™ Reagent (Thermo Fisher Scientific Inc., USA), based on previously described methods [10]. Afterwards, each cell suspension was mixed with TRIzol™ Reagent in a 3:1 ratio to lyse the cells. The total RNA from the lysed samples was purified using the Direct-zol™ RNA Miniprep Kit (Zymo Research, USA), according to the manufacturer's instructions. Total RNA quality control was assessed using the BioAnalyzer 2100 - RNA 6000 Pico kit (Agilent, USA) following the manufacturer's instructions, and the total RNA was quantified with the Qubit 3.0 fluorometer - RNA High Sensitivity Assay (Thermo Fisher Scientific Inc., USA).

Transcriptomic Profile – RNA Sequencing: Ion Torrent sequencing libraries were prepared according to the AmpliSeq™ Transcriptome Human Gene Expression Kit (Thermo Fisher Scientific Inc., USA) protocol, following the manufacturer's instructions. Briefly, 10 ng of total RNA was reverse transcribed, and the resulting cDNA was amplified for 12 cycles by adding PCR Master Mix and the AmpliSeq Human transcriptome gene expression primer pool. Amplicons were digested with the proprietary FuPa enzyme, then barcoded adapters were ligated onto the target amplicons. The library amplicons were bound to magnetic beads, and residual reaction components were washed off. Libraries were amplified, re-purified, and individually quantified using Agilent TapeStation High Sensitivity tape. Individual libraries were diluted to a 50 pM concentration and pooled equally. Emulsion PCR, templating and 540 chip loading were performed with an Ion Chef Instrument (Thermo Fisher Scientific Inc., USA). Sequencing was performed on an Ion S5 Prime™ sequencer (Thermo Fisher Scientific Inc., USA).

Transcriptomic Profile – Bioinformatic Analysis: The data were processed using the Ion Torrent platform-specific pipeline software Torrent Suite version 5.18 to generate sequence reads, trim adapter sequences, filter and remove poor signal reads, and split the reads according to the barcode. FASTQ and BAM files were generated using the Torrent Suit plugin FileExporter version 5.18. Primary automated analysis for AmpliSeq sequencing data of all samples was performed using the ampliSeqRNA plugin version 5.18 (target region "hg19_AmpliSeq_Transcriptome_21K_v1). Plugin reports were normalized considering transcript counts in spreadsheet file formats. The files containing normalized data were uploaded to Affymetrix's Transcriptome Analysis Console (TAC) Software (version 4.0.3.14, Thermo Fisher Scientific Inc., USA) for differential expression analysis. The TAC software provided principal component analysis (PCA) and volcano plots, and hierarchical clustering for comparison of 2D, hPLMA and Matrigel conditions. Differentially expressed genes (DEGs) were selected considering p-value <0.01, FDR p-value <0.05 and absolute fold change ≥ 2. Functional enrichment analysis of the top 20 DEGs upregulated in each condition was performed using the g:Profiler tool (https://biit.cs.ut.ee/gprofiler/, version e113_eg59_p19_f6a03c19), considering gene ontology (GO) terms for biological processes (BP), molecular function (MF) and cellular component (CC). Function clustering of all the DEGs in each condition was performed using the DAVID Bioinformatics tool, considering the GO terms for BP [79,80]. These results were also represented in an alluvial plot created in the SRplot platform [81]. Cell-type enrichment of gene signatures was assessed with the Database of Immune Cell Expression (DICE) CellTypeScore tool, which scores and visualizes the combined expression of input genes across DICE immune cell subsets [82]. The main DEGs associated with immunomodulation were integrated in the SIGnaling Network Open Resource (SIGNOR) platform (version 4.0) to create networks of functional interactions between these genes. A score of 0.6 was applied to consider only interactions with strong supporting evidence of the functional interactions [83].

Statistical Analysis: All the data are expressed as mean ± standard deviation (SD) of three replicates per assay of three independent assays, unless otherwise stated. To compare the metabolic activity of different hPLMA and Matrigel batches, the coefficient of variation (CV), i.e., the ratio of the standard deviation to the mean, was determined to have a normalized measure of dispersion. The data were statistically analyzed using GraphPad Prism version 6.05 for Windows (GraphPad Software, USA), always using a significance of $p < 0.05$.

CRediT authorship contribution statement

Mariana M. Dias: Formal analysis, Investigation, Writing – original draft. **Ana T. Rufino:** Supervision, Validation, Writing – review & editing. **Rui Vitorino:** Formal analysis. **Catarina A. Custódio:** Conceptualization, Funding acquisition, Supervision, Writing – review & editing. **João F. Mano:** Formal analysis, Funding acquisition, Resources, Supervision, Writing – review & editing.

Declaration of competing interest

The authors declare that they have no known competing financial interests or personal relationships that could have appeared to influence the work reported in this paper.

Acknowledgements

This work was funded by the Portuguese Foundation for Science and Technology (FCT), Lisbon, Portugal, with the individual contract of C.A.C. (2020.01647.CEECIND) and by the Programa Operacional Competitividade e Internacionalização in the component FEDER (COMPETE2030-FEDER-00836800). This work was also within the scope of the project CICECO Aveiro Institute of Materials, UID/50011/2025 (DOI 10.54499/UID/50011/2025) & LA/P/0006/2020 (DOI 10.54499/LA/P/0006/2020), financed by national funds through the FCT/MCTES (PIDDAC). The authors wish to acknowledge the European Union's Horizon research and innovation program under grant agreement No 101191729, project m2M, and the European Research Council for project 'REBORN' (ERC-2019-AdG-883370). C.A.C. acknowledges the project Advancing Disease Modeling and Drug Screening with a Fully Human 3D-Printed Cardiac Microphysiological System (DOI https://doi.org/10.54499/2023.17280.ICDT). M.D. also acknowledges the support from the FCT on her PhD grant reference 2025.01150. BDANA. The authors acknowledge the support of the i3S Genomics Scientific Platform for the transcriptomic laboratory processing.

Appendix A. Supplementary data

Supplementary data to this article can be found online at https://doi.org/10.1016/j.mtbio.2026.103443.

Data availability

Data will be made available on request.

References

[1] C.Y. Tay, M.S. Muthu, S.L. Chia, K.T. Nguyen, S.-S. Feng, D.T. Leong, Reality check for nanomaterial-mediated therapy with 3D biomimetic culture systems, Adv. Funct. Mater. 26 (2016) 4046–4065, https://doi.org/10.1002/adfm.201600476.
[2] H.K. Kleinman, G.R. Martin, Matrigel: basement membrane matrix with biological activity, Semin. Cancer Biol. 15 (2005) 378–386, https://doi.org/10.1016/j.semcancer.2005.05.004.
[3] E.A. Aisenbrey, W.L. Murphy, Synthetic alternatives to matrigel, Nat. Rev. Mater. 5 (2020) 539–551, https://doi.org/10.1038/s41578-020-0199-8.
[4] H.K. Kleinman, Preparation of basement membrane components from EHS tumors, Curr. Protoc. Cell Biol. 00 (1998), https://doi.org/10.1002/0471143030.cb1002s00.
[5] R. Fridman, G. Giaccone, T. Kanemoto, G.R. Martin, A.F. Gazdar, J.L. Mulshine, Reconstituted basement membrane (matrigel) and laminin can enhance the tumorigenicity and the drug resistance of small cell lung cancer cell lines, Proc. Natl. Acad. Sci. U. S. A. 87 (1990) 6698–6702, https://doi.org/10.1073/pnas.87.17.6698.
[6] H. Liu, J. Bockhorn, R. Dalton, Y.-F. Chang, D. Qian, L.A. Zitzow, M.F. Clarke, G. L. Greene, Removal of lactate dehydrogenase-elevating virus from human-in-mouse breast tumor xenografts by cell-sorting, J. Virol. Methods 173 (2011) 266–270, https://doi.org/10.1016/j.jviromet.2011.02.015.
[7] S.E. Hocevar, L. Liu, R.K. Duncan, Matrigel is required for efficient differentiation of isolated, stem cell-derived otic vesicles into inner ear organoids, Stem Cell Res. 53 (2021) 102295, https://doi.org/10.1016/j.scr.2021.102295.
[8] C.S. Hughes, L.M. Postovit, G.A. Lajoie, Matrigel: a complex protein mixture required for optimal growth of cell culture, Proteomics 10 (2010) 1886–1890, https://doi.org/10.1002/pmic.200900758.
[9] J. Berg, Clean bioprinting - fabrication of 3D organ models devoid of animal components, ALTEX (2020), https://doi.org/10.14573/altex.2009151.
[10] R. Ferretti, A. Baldassarre, E.D. Billy, A. M Carcaboso, A. Moore, A. Carai, A. Mastronuzzi, A. Masotti, M. Vinci, Tumor cell invasion into matrigel: optimized protocol for RNA extraction, Biotechniques 70 (2021) 327–335, https://doi.org/10.2144/btn-2021-0001.
[11] T. Schmitt, N. Kajave, H.H. Cai, L. Gu, M. Albanna, V. Kishore, In vitro characterization of xeno-free clinically relevant human collagen and its applicability in cell-laden 3D bioprinting, J. Biomater. Appl. 35 (2021) 912–923, https://doi.org/10.1177/0885328220959162.
[12] G. Mazza, K. Rombouts, A. Rennie Hall, L. Urbani, T. Vinh Luong, W. Al-Akkad, L. Longato, D. Brown, P. Maghsoudlou, A.P. Dhillon, B. Fuller, B. Davidson, K. Moore, D. Dhar, P. De Coppi, M. Malago, M. Pinzani, Decellularized human liver as a natural 3D-scaffold for liver bioengineering and transplantation, Sci. Rep. 5 (2015) 13079, https://doi.org/10.1038/srep13079.
[13] I.A. Deus, S.C. Santos, C.A. Custódio, J.F. Mano, Designing highly customizable human based platforms for cell culture using proteins from the amniotic membrane, Biomater. Adv. 134 (2022) 112574, https://doi.org/10.1016/j.msec.2021.112574.
[14] J.P.M. Sousa, I.A. Deus, C.F. Monteiro, C.A. Custódio, J. Gil, L. Papadimitriou, A. Ranella, E. Stratakis, J.F. Mano, P.A.A.P. Marques, Amniotic membrane-derived multichannel hydrogels for neural tissue repair, Adv Healthc Mater 13 (2024) 2400522, https://doi.org/10.1002/adhm.202400522.
[15] M. Kirsch, L. Birnstein, I. Pepelanova, W. Handke, J. Rach, A. Seltsam, T. Scheper, A. Lavrentieva, Gelatin-Methacryloyl (GelMA) formulated with human platelet lysate supports mesenchymal stem cell proliferation and differentiation and enhances the Hydrogel's mechanical properties, Bioengineering 6 (2019) 76, https://doi.org/10.3390/bioengineering6030076.
[16] M. Kirsch, J. Rach, W. Handke, A. Seltsam, I. Pepelanova, S. Strauß, P. Vogt, T. Scheper, A. Lavrentieva, Comparative analysis of mesenchymal stem cell cultivation in fetal calf serum, human serum, and platelet lysate in 2D and 3D systems, Front. Bioeng. Biotechnol. 8 (2021) 598389, https://doi.org/10.3389/fbioe.2020.598389.
[17] S.C. Santos, C.A. Custódio, J.F. Mano, Photopolymerizable platelet lysate hydrogels for customizable 3D cell culture platforms, Adv Healthc Mater 7 (2018) 1800849, https://doi.org/10.1002/adhm.201800849.
[18] C.F. Monteiro, M.C. Gomes, P. Bharmoria, M.G. Freire, J.A.P. Coutinho, C. A. Custódio, J.F. Mano, Human platelet lysate-derived nanofibrils as building blocks to produce free-standing membranes for cell self-aggregation, ACS Nano 18 (2024) 15815–15830, https://doi.org/10.1021/acsnano.4c02790.
[19] S.C. Santos, C.A. Custódio, J.F. Mano, Photocrosslinkable microgels derived from human platelet lysates: injectable biomaterials for cardiac cell culture, Biomater. Sci. 12 (2024) 3112–3123, https://doi.org/10.1039/D3BM01933K.
[20] C.F. Monteiro, C.R. Almeida, C.A. Custódio, J.F. Mano, Modeling 3D tumor invasiveness to modulate macrophage phenotype in a human-based Hydrogel platform, Macromol. Biosci. 70 (2024) 2400227, https://doi.org/10.1002/mabi.202400227.
[21] C.F. Monteiro, S.C. Santos, C.A. Custódio, J.F. Mano, Human platelet lysates-based hydrogels: a novel personalized 3D platform for spheroid invasion assessment, Adv Sci 7 (2020) 1902398, https://doi.org/10.1002/advs.201902398.
[22] P. Zhang, A. Policha, T. Tulenko, P. DiMuzio, Autologous human plasma in stem cell culture and cryopreservation in the creation of a tissue-engineered vascular graft, J. Vasc. Surg. 63 (2016) 805–814, https://doi.org/10.1016/j.jvs.2014.10.015.
[23] A. Golunova, J. Jaroš, V. Jurtíková, I. Kotelnikov, J. Kotek, H. Hlídková, L. Streit, A. Hampl, F. Rypáček, V. Proks, N-(2-Hydroxypropyl) methacrylamide based cryogels – synthesis and biomimetic modification for stem cell applications, Physiol. Res. (2015) S19–S27, https://doi.org/10.33549/physiolres.933134.
[24] H. Li, Y.S. Wong, F. Wen, K.W. Ng, G.K.L. Ng, S.S. Venkatraman, F.Y.C. Boey, L. P. Tan, Human mesenchymal stem-cell behaviour on direct laser micropatterned electrospun scaffolds with hierarchical structures, Macromol. Biosci. 13 (2013) 299–310, https://doi.org/10.1002/mabi.201200318.
[25] M.A. Serban, Y. Liu, G.D. Prestwich, Effects of extracellular matrix analogues on primary human fibroblast behavior, Acta Biomater. 4 (2008) 67–75, https://doi.org/10.1016/j.actbio.2007.09.006.
[26] S.S. Soofi, J.A. Last, S.J. Liliensiek, P.F. Nealey, C.J. Murphy, The elastic modulus of Matrigel™ as determined by atomic force microscopy, J. Struct. Biol. 167 (2009) 216–219, https://doi.org/10.1016/j.jsb.2009.05.005.
[27] J. Reed, W.J. Walczak, O.N. Petzold, J.K. Gimzewski, In situ mechanical interferometry of Matrigel™ films, Langmuir 25 (2009) 36–39, https://doi.org/10.1021/la8033098.
[28] N.K. Karamanos, A.D. Theocharis, Z. Piperigkou, D. Manou, A. Passi, S. S. Skandalis, D.H. Vynios, V. Orian-Rousseau, S. Ricard-Blum, C.E.H. Schmelzer,

L. Duca, M. Durbeej, N.A. Afratis, L. Troeberg, M. Franchi, V. Masola, M. Onisto, A guide to the composition and functions of the extracellular matrix, FEBS J. 288 (2021) 6850–6912, https://doi.org/10.1111/febs.15776.
[29] J.M. Gomes, S.S. Silva, E.M. Fernandes, F.C.M. Lobo, M. Martín-Pastor, P. Taboada, R.L. Reis, Silk fibroin/cholinium gallate-based architectures as therapeutic tools, Acta Biomater. 147 (2022) 168–184, https://doi.org/10.1016/j.actbio.2022.05.020.
[30] F. Bisconti, B. Vilardo, G. Corallo, F. Scalera, G. Gigli, A. Chiocchetti, A. Polini, F. Gervaso, An assist for arthritis studies: a 3D cell culture of human fibroblast-like synoviocytes by encapsulation in a chitosan-based hydrogel, Adv. Ther. (2024) 2400166, https://doi.org/10.1002/adtp.202400166.
[31] C. Luckert, C. Schulz, N. Lehmann, M. Thomas, U. Hofmann, S. Hammad, J. G. Hengstler, A. Braeuning, A. Lampen, S. Hessel, Comparative analysis of 3D culture methods on human HepG2 cells, Arch. Toxicol. 91 (2017) 393–406, https://doi.org/10.1007/s00204-016-1677-z.
[32] L. Yu, Y. Wu, J. Liu, B. Li, B. Ma, Y. Li, Z. Huang, Y. He, H. Wang, Z. Wu, G. Qiu, 3D culture of bone marrow-derived mesenchymal stem cells (BMSCs) could improve bone regeneration in 3D-Printed porous Ti6Al4V scaffolds, Stem Cells Int 2018 (2018) 13, https://doi.org/10.1155/2018/2074021.
[33] A.P. Wong, S.L. Cortez, W.H. Baricos, Role of plasmin and gelatinase in extracellular matrix degradation by cultured rat mesangial cells, Am J Physiol Renal Physiol 263 (1992) F1112–F1118, https://doi.org/10.1152/ajprenal.1992.263.6.F1112.
[34] Y.H. Song, S.H. Shon, M. Shan, A.D. Stroock, C. Fischbach, Adipose-derived stem cells increase angiogenesis through matrix metalloproteinase-dependent collagen remodeling, Integr. Biol. 8 (2016) 205–215, https://doi.org/10.1039/C5IB00277J.
[35] K.M. Gillette, K. Forbes, I. Sehgal, Detection of matrix metalloproteinases (MMP), tissue inhibitor of metalloproteinase-2, urokinase and plasminogen activator inhibitor-1 within matrigel and growth factor-reduced matrigel basement membrane, Tumori 89 (2003) 421–425, https://doi.org/10.1177/030089160308900415.
[36] C.F. Monteiro, C.A. Custódio, J.F. Mano, Bioengineering a humanized 3D tri-culture osteosarcoma model to assess tumor invasiveness and therapy response, Acta Biomater. 134 (2021) 204–214, https://doi.org/10.1016/j.actbio.2021.07.034.
[37] S.C. Santos, C.A. Custódio, J.F. Mano, Human protein-based porous scaffolds as platforms for xeno-free 3D cell culture, Adv Healthc Mater 11 (2022) e2102383, https://doi.org/10.1002/adhm.202102383.
[38] Corning Incorporated, Corning® Matrigel® Matrix - Frequently Asked Questions, 2021. Corning, NY, USA, https://www.corning.com/catalog/cls/documents/faqs/CLS-DL-CC-026.pdf. (Accessed 10 March 2026).
[39] Q. Li, B.E. Uygun, S. Geerts, S. Ozer, M. Scalf, S.E. Gilpin, H.C. Ott, M.L. Yarmush, L.M. Smith, N.V. Welham, B.L. Frey, Proteomic analysis of naturally-sourced biological scaffolds, Biomaterials 75 (2016) 37–46, https://doi.org/10.1016/j.biomaterials.2015.10.011.
[40] X. Liu, Y. Qiao, J. Chen, G. Ge, Basement membrane promotes tumor development by attenuating T cell activation, J. Mol. Cell Biol. 14 (2022) e006, https://doi.org/10.1093/jmcb/mjac006.
[41] K. Schneeberger, B. Spee, P. Costa, N. Sachs, H. Clevers, J. Malda, Converging biofabrication and organoid technologies: the next frontier in hepatic and intestinal tissue engineering? Biofabrication 9 (2017) 013001 https://doi.org/10.1088/1758-5090/aa6121.
[42] J. Shi, Q. Li, M. Sheng, M. Zheng, M. Yu, L. Zhang, The role of TLR4 in M1 macrophage-induced epithelial-mesenchymal transition of peritoneal mesothelial cells, Cell. Physiol. Biochem. 40 (2016) 1538–1548, https://doi.org/10.1159/000453204.
[43] C. Liu, D. Chu, K. Kalantar-Zadeh, J. George, H.A. Young, G. Liu, Cytokines: from clinical significance to quantification, Adv Sci 8 (2021) 2004433, https://doi.org/10.1002/advs.202004433.
[44] J. Cho, S.I. Lim, B.S. Yang, Y.S. Hahn, I. Kwon, Generation of therapeutic protein variants with the human serum albumin binding capacity via site-specific fatty acid conjugation, Sci. Rep. 7 (2017) 18041, https://doi.org/10.1038/s41598-017-18029-y.
[45] C.M. Walsh, J.K. Wychowaniec, L. Costello, D.F. Brougham, D. Dooley, An in vitro and Ex vivo analysis of the potential of GelMA hydrogels as a therapeutic platform for preclinical spinal cord injury, Adv. Healthcare Mater. 12 (2023) 2300951, https://doi.org/10.1002/adhm.202300951.
[46] M.C. Regier, S.I. Montanez-Sauri, M.P. Schwartz, W.L. Murphy, D.J. Beebe, K. E. Sung, The influence of biomaterials on cytokine production in 3D cultures, Biomacromolecules 18 (2017) 709–718, https://doi.org/10.1021/acs.biomac.6b01469.
[47] A. Noël, M.C. De Pauw-Gillet, G. Purnell, B. Nusgens, C.M. Lapiere, J.M. Foidart, Enhancement of tumorigenicity of human breast adenocarcinoma cells in nude mice by matrigel and fibroblasts, Br. J. Cancer 68 (1993) 909–915.
[48] A. Passaniti, H.K. Kleinman, G.R. Martin, Matrigel: history/background, uses, and future applications, J. Cell Commun. Signal. 16 (2022) 621–626, https://doi.org/10.1007/s12079-021-00643-1.
[49] A.R. Albig, T.G. Roy, D.J. Becenti, W.P. Schiemann, Transcriptome analysis of endothelial cell gene expression induced by growth on matrigel matrices: identification and characterization of MAGP-2 and Lumican as novel regulators of angiogenesis, Angiogenesis 10 (2007) 197–216, https://doi.org/10.1007/s10456-007-9075-z.
[50] D. Choi, A.M. Gonzalez-Suarez, M.G. Dumbrava, M. Medlyn, J.M. de Hoyos-Vega, F. Cichocki, J.S. Miller, L. Ding, M. Zhu, G. Stybayeva, A. Gaspar-Maia, D. D. Billadeau, W.W. Ma, A. Revzin, Microfluidic organoid cultures derived from pancreatic cancer biopsies for personalized testing of chemotherapy and immunotherapy, Adv. Sci. 11 (2024) 2303088, https://doi.org/10.1002/advs.202303088.
[51] R. Kerslake, B. Belay, S. Panfilov, M. Hall, I. Kyrou, H.S. Randeva, J. Hyttinen, E. Karteris, C. Sisu, Transcriptional landscape of 3D vs. 2D ovarian cancer cell models, Cancers 15 (2023) 3350, https://doi.org/10.3390/cancers15133350.
[52] G.G. Giobbe, C. Crowley, C. Luni, S. Campinoti, M. Khedr, K. Kretzschmar, M.M. De Santis, E. Zambaiti, F. Michielin, L. Meran, Q. Hu, G. Van Son, L. Urbani, A. Manfredi, M. Giomo, S. Eaton, D. Cacchiarelli, V.S.W. Li, H. Clevers, P. Bonfanti, N. Elvassore, P. De Coppi, Extracellular matrix hydrogel derived from decellularized tissues enables endodermal organoid culture, Nat. Commun. 10 (2019) 5658, https://doi.org/10.1038/s41467-019-13605-4.
[53] S. Kim, S. Min, Y.S. Choi, S.-H. Jo, J.H. Jung, K. Han, J. Kim, S. An, Y.W. Ji, Y.-G. Kim, S.-W. Cho, Tissue extracellular matrix hydrogels as alternatives to matrigel for culturing gastrointestinal organoids, Nat. Commun. 13 (2022) 1692, https://doi.org/10.1038/s41467-022-29279-4.
[54] L. Magré, M.M.A. Verstegen, S. Buschow, L.J.W. van der Laan, M. Peppelenbosch, J. Desai, Emerging organoid-immune co-culture models for cancer research: from oncoimmunology to personalized immunotherapies, J. Immunother. Cancer 11 (2023), https://doi.org/10.1136/jitc-2022-006290.
[55] J. Li, T. Guo, Y. Li, Q. Wang, Y. Du, R. Li, J. Lin, J. Fu, X. Chen, S. Luo, Adipose stem cells regulate lipid metabolism by upregulating mitochondrial fatty acid β-oxidation in macrophages to improve the retention rate of transplanted fat, Stem Cell Res. Ther. 15 (2024) 328, https://doi.org/10.1186/s13287-024-03953-4.
[56] S. Ceccarelli, P. Pontecorvi, E. Anastasiadou, C. Napoli, C. Marchese, Immunomodulatory effect of adipose-derived stem cells: the cutting edge of clinical application, Front. Cell Dev. Biol. 8 (2020) 236, https://doi.org/10.3389/fcell.2020.00236.
[57] Y. Mitamura, S. Nunomura, M. Furue, K. Izuhara, IL-24: a new player in the pathogenesis of pro-inflammatory and allergic skin diseases, Allergol. Int. 69 (2020) 405–411, https://doi.org/10.1016/j.alit.2019.12.003.
[58] C. Dessels, M.A. Ambele, M.S. Pepper, The effect of medium supplementation and serial passaging on the transcriptome of human adipose-derived stromal cells expanded in vitro, Stem Cell Res. Ther. 10 (2019) 253, https://doi.org/10.1186/s13287-019-1370-2.
[59] N.C. Talbot, T.J. Caperna, Proteome array identification of bioactive soluble proteins/peptides in matrigel: relevance to stem cell responses, Cytotechnology 67 (2015) 873–883, https://doi.org/10.1007/s10616-014-9727-y.
[60] S. Wolbank, A. Peterbauer, M. Fahrner, S. Hennerbichler, M. Van Griensven, G. Stadler, H. Redl, C. Gabriel, Dose-dependent immunomodulatory effect of human stem cells from amniotic membrane: a comparison with human mesenchymal stem cells from adipose tissue, Tissue Eng. 13 (2007) 1173–1183, https://doi.org/10.1089/ten.2006.0313.
[61] M. Mahmoud, M. Abdel-Rasheed, E.R. Galal, R.R. El-Awady, Factors defining human Adipose Stem/stromal cell immunomodulation in vitro, Stem Cell Rev. Rep. 20 (2024) 175–205, https://doi.org/10.1007/s12015-023-10654-7.
[62] M. Madrigal, K.S. Rao, N.H. Riordan, A review of therapeutic effects of mesenchymal stem cell secretions and induction of secretory modification by different culture methods, J. Transl. Med. 12 (2014) 260, https://doi.org/10.1186/s12967-014-0260-8.
[63] D.-L. Dong, G.-Z. Jin, YAP and ECM stiffness: key drivers of adipocyte differentiation and lipid accumulation, Cells 13 (2024) 1905, https://doi.org/10.3390/cells13221905.
[64] C. Kim, J.L. Young, A.W. Holle, K. Jeong, L.G. Major, J.H. Jeong, Z.M. Aman, D.-W. Han, Y. Hwang, J.P. Spatz, Y.S. Choi, Stem cell mechanosensation on gelatin methacryloyl (GelMA) stiffness gradient hydrogels, Ann. Biomed. Eng. 48 (2020) 893–902, https://doi.org/10.1007/s10439-019-02428-5.
[65] B.H. Marcon, P. Shigunov, L. Spangenberg, I.T. Pereira, A.M. De Aguiar, R. Amorín, C.K. Rebelatto, A. Correa, B. Dallagiovanna, Cell cycle genes are downregulated after adipogenic triggering in human adipose tissue-derived stem cells by regulation of mRNA abundance, Sci. Rep. 9 (2019) 5611, https://doi.org/10.1038/s41598-019-42005-3.
[66] P. Yavvari, A. Laporte, L. Elomaa, F. Schraufstetter, I. Pacharzina, A.D. Daberkow, A. Hoppensack, M. Weinhart, 3D-Cultured vascular-like networks enable validation of vascular disruption properties of drugs in vitro, Front. Bioeng. Biotechnol. 10 (2022), https://doi.org/10.3389/fbioe.2022.888492.
[67] S. Chowdhury, K. Beeton, Z. Wallace, M. Moore, G.L. Bidwell, A.V. Janorkar, Extending the three-dimensional culture of adipocytes through surface coatings, Bioengineering 12 (2025) 266, https://doi.org/10.3390/bioengineering12030266.
[68] D.C. Ferreira Golbert, E. Correa-de-Santana, M. Ribeiro-Alves, A.T.R. de Vasconcelos, W. Savino, ITGA6 gene silencing by RNA interference modulates the expression of a large number of cell migration-related genes in human thymic epithelial cells, BMC Genom. 14 (2013) S3, https://doi.org/10.1186/1471-2164-14-S6-S3.
[69] Y.-M. Yang, X.-H. Dong, W.-C. Ma, L.-H. Guan, Y.-H. Wang, X.-H. Huang, J.-F. Chen, X. Zhao, Proliferation, differentiation and immunoregulatory capacities of brown and white adipose-derived stem cells from young and aged mice, Int. J. Stem Cells 13 (2020) 246–256, https://doi.org/10.15283/ijsc20019.
[70] G. Ren, X. Zhao, L. Zhang, J. Zhang, A. L'Huillier, W. Ling, A.I. Roberts, A.D. Le, S. Shi, C. Shao, Y. Shi, Inflammatory cytokine-induced intercellular adhesion Molecule-1 and vascular cell adhesion Molecule-1 in mesenchymal stem cells are critical for immunosuppression, J. Immunol. 184 (2010) 2321–2328, https://doi.org/10.4049/jimmunol.0902023.
[71] L. Cao, P. Zhang, J. Li, M. Wu, LAST, a c-Myc-inducible long noncoding RNA, cooperates with CNBP to promote CCND1 mRNA stability in human cells, eLife 6 (2017) e30433, https://doi.org/10.7554/eLife.30433.

[72] K.J. Opperman, B. Grill, RPM-1 is localized to distinct subcellular compartments and regulates axon length in GABAergic motor neurons, Neural Dev. 9 (2014) 10, https://doi.org/10.1186/1749-8104-9-10.
[73] N. Rashidi, N.S. Harasymowicz, A. Savadipour, N. Steward, R. Tang, S. Oswald, F. Guilak, PIEZO1-mediated mechanotransduction regulates collagen synthesis on nanostructured 2D and 3D models of fibrosis, Acta Biomater. 193 (2025) 242–254, https://doi.org/10.1016/j.actbio.2024.12.034.
[74] R. Laczko, K. Csiszar, Lysyl oxidase (LOX): functional contributions to signaling pathways, Biomolecules 10 (2020) 1093, https://doi.org/10.3390/biom10081093.
[75] X. Li, B. Cho, R. Martin, M. Seu, C. Zhang, Z. Zhou, J.S. Choi, X. Jiang, L. Chen, G. Walia, J. Yan, M. Callanan, H. Liu, K. Colbert, J. Morrissette-McAlmon, W. Grayson, S. Reddy, J.M. Sacks, H.-Q. Mao, Nanofiber-hydrogel composite–mediated angiogenesis for soft tissue reconstruction, Sci. Transl. Med. 11 (2019) e6210, https://doi.org/10.1126/scitranslmed.aau6210.
[76] C.R. Correia, T.C. Santos, R.P. Pirraco, M.T. Cerqueira, A.P. Marques, R.L. Reis, J. F. Mano, In vivo osteogenic differentiation of stem cells inside compartmentalized capsules loaded with co-cultured endothelial cells, Acta Biomater. 53 (2017) 483–494, https://doi.org/10.1016/j.actbio.2017.02.007.
[77] O. Gavet, J. Pines, Progressive activation of CyclinB1-Cdk1 coordinates entry to mitosis, Dev. Cell 18 (2010) 533–543, https://doi.org/10.1016/j.devcel.2010.02.013.
[78] M. Genin, F. Clement, A. Fattaccioli, M. Raes, C. Michiels, M1 and M2 macrophages derived from THP-1 cells differentially modulate the response of cancer cells to etoposide, BMC Cancer 15 (2015) 577, https://doi.org/10.1186/s12885-015-1546-9.
[79] D.W. Huang, B.T. Sherman, R.A. Lempicki, Systematic and integrative analysis of large gene lists using DAVID bioinformatics resources, Nat. Protoc. 4 (2009) 44–57, https://doi.org/10.1038/nprot.2008.211.
[80] B.T. Sherman, M. Hao, J. Qiu, X. Jiao, M.W. Baseler, H.C. Lane, T. Imamichi, W. Chang, DAVID: a web server for functional enrichment analysis and functional annotation of gene lists (2021 update), Nucleic Acids Res. 50 (2022) W216–W221, https://doi.org/10.1093/nar/gkac194.
[81] D. Tang, M. Chen, X. Huang, G. Zhang, L. Zeng, G. Zhang, S. Wu, Y. Wang, SRplot: a free online platform for data visualization and graphing, PLoS One 18 (2023) e0294236, https://doi.org/10.1371/journal.pone.0294236.
[82] B.J. Schmiedel, D. Singh, A. Madrigal, A.G. Valdovino-Gonzalez, B.M. White, J. Zapardiel-Gonzalo, B. Ha, G. Altay, J.A. Greenbaum, G. McVicker, G. Seumois, A. Rao, M. Kronenberg, B. Peters, P. Vijayanand, Impact of genetic polymorphisms on human immune cell gene expression, Cell 175 (2018) 1701–1715.e16, https://doi.org/10.1016/j.cell.2018.10.022.
[83] P. Lo Surdo, M. Iannuccelli, K. Karis, E. Meo, P. Omidi, M. Tosoni, S. Graziosi, S. Panni, M.T. Fiorillo, L. Licata, F. Sacco, B.M. Gyori, L. Perfetto, Signor 4.0: the 2025 update with focus on phosphorylation data, Nucleic Acids Res. 54 (2026) D682–D690, https://doi.org/10.1093/nar/gkaf1237.